

คาร์บอนไดออกไซด์ไฮโดรเจนชั้นบนตัวเร่งปฏิกิริยา Co/SBA-15 และ Co/SBA-16
ที่สังเคราะห์ด้วยซีเรีย

นางสาวจิตรารัตน์ เครือทิม

วิทยานิพนธ์นี้เป็นส่วนหนึ่งของการศึกษาตามหลักสูตรปริญญาวิศวกรรมศาสตรมหาบัณฑิต
สาขาวิชาวิศวกรรมเคมี ภาควิชาวิศวกรรมเคมี
คณะวิศวกรรมศาสตร์ จุฬาลงกรณ์มหาวิทยาลัย
ปีการศึกษา 2556
ลิขสิทธิ์ของจุฬาลงกรณ์มหาวิทยาลัย

บทคัดย่อและแฟ้มข้อมูลฉบับเต็มของวิทยานิพนธ์ตั้งแต่ปีการศึกษา 2554 ที่ให้บริการในคลังปัญญาจุฬาฯ (CUIR)
เป็นแฟ้มข้อมูลของนิสิตเจ้าของวิทยานิพนธ์ที่ส่งผ่านทางบัณฑิตวิทยาลัย

The abstract and full text of theses from the academic year 2011 in Chulalongkorn University Intellectual Repository (CUIR)
are the thesis authors' files submitted through the Graduate School.

CO₂ HYDROGENATION OVER CO/SBA-15 AND Co/SBA-16 CATALYSTS
PROMOTED WITH CERIA

Miss Jitraporn Kruatim

A Thesis Submitted in Partial Fulfillment of the Requirements
for the Degree of Master of Engineering Program in Chemical Engineering

Department of Chemical Engineering

Faculty of Engineering

Chulalongkorn University

Academic Year 2013

Copyright of Chulalongkorn University

จิตรภรณ์ เครือทิม : คาร์บอนไดออกไซด์ไฮโดรจิเนชันบนตัวเร่งปฏิกิริยา Co/SBA-15 และ Co/SBA-16 ที่ส่งเสริมด้วยซีเรีย. (CO₂ HYDROGENATION OVER CO/SBA-15 AND CO/SBA-16 CATALYSTS PROMOTED WITH CERIA) อ.ที่ปรึกษา
 วิทยานิพนธ์หลัก : รศ.ดร.บรรเจิด จงสมจิตร, 94 หน้า.

งานวิจัยนี้ทำการเตรียมตัวเร่งปฏิกิริยา Co/SBA-15 และ Co/SBA-16 ใช้โคบอลต์ 20% โดยน้ำหนัก โดยเตรียมด้วยวิธีการฝัง มีการประยุกต์ใช้การฝังในระบบสุญญากาศและการใช้อัลตราซาวนด์หลังการเคลือบฝัง นอกจากนี้ยังมีการสนับสนุนซีเรียบนตัวเร่งปฏิกิริยาโคบอลต์ด้วยวิธีการเคลือบฝังร่วม (co-impregnation) และวิธีการเคลือบฝังแบบเป็นลำดับขั้นตอน (sequential-impregnation) ตัวเร่งปฏิกิริยาจะถูกทดสอบคุณลักษณะด้วย N₂ physisorption, SAXRD, XRD, SEM/EDX, TEM และ TPR จากผลการทดลองพบว่าทั้งการฝังในระบบสุญญากาศและการใช้อัลตราซาวนด์หลังการฝังช่วยเพิ่มการกระจายตัวของโคบอลต์บนตัวเร่งปฏิกิริยา Co/SBA-15 แต่การฝังในระบบสุญญากาศเท่านั้นที่เหมาะสมสำหรับตัวเร่งปฏิกิริยา Co/SBA-16 หลังจากกระบวนการรีดักชัน ผลจากการวิเคราะห์ด้วยXRDไม่พบสารประกอบโคบอลต์ซัลไฟด์ ทั้งสองกระบวนการสามารถลดอันตรกิริยา จึงทำให้ความว่องไวของปฏิกิริยาคาร์บอนไดออกไซด์ไฮโดรจิเนชันเพิ่มขึ้น นอกจากนี้ยังพบว่า การสนับสนุนด้วยซีเรียทำให้ความสามารถในการรีดิวซ์เพิ่มขึ้น และช่วยลดอันตรกิริยา เป็นผลให้ประสิทธิภาพเชิงเร่งดีขึ้น อย่างไรก็ตาม การสนับสนุนด้วยซีเรียพร้อมกับกระบวนการหลังการเคลือบฝังไม่เพิ่มประสิทธิภาพเชิงเร่ง ควรเลือกเพียงการสนับสนุนหรือกระบวนการหลังการเคลือบฝังเพียงอย่างใดอย่างหนึ่งเท่านั้น

ภาควิชาวิศวกรรมเคมี..... ลายมือชื่อนิติดี

สาขาวิชาวิศวกรรมเคมี..... ลายมือชื่อ อ.ที่ปรึกษาวิทยานิพนธ์หลัก

ปีการศึกษา2556.....

5470140421 : MAJOR CHEMICAL ENGINEERING

KEYWORDS : COBALT CATALYST / SBA-15 / SBA-16 / TPR / DISPERSION

JITTRAPORN KRUTIM : CO₂ HYDROGENATION OVER CO/SBA-15 AND
CO/SBA-16 CATALYSTS PROMOTED WITH CERIA. ADVISOR : ASSOC. PROF.
BUNJERD JONGSOMJIT, Ph.D., 94 pp.

In this study, the Co/SBA-15 and Co/SBA-16 having 20 wt% of cobalt were prepared by the conventional impregnation method. Then, the post-impregnation treatment such as vacuum and ultrasound treatments were applied. Moreover, Ce-promoted cobalt catalysts were also prepared by co-impregnation and sequential impregnation method. The catalyst samples were characterized by means of N₂ physisorption, small angle X-ray diffraction (SAXRD), wide angle X-ray diffraction (XRD), scanning electron microscopy and energy dispersive X-ray spectroscopy (SEM/EDX), transmission electron spectroscopy (TEM), and temperature-programmed reduction (TPR). It was found that the vacuum and ultrasound treatments can apparently enhance the dispersion of Co/SBA-15 catalysts, whereas only vacuum treatment was suitable for Co/SBA-16. After reduction, no cobalt-silicate compound was detected based on XRD measurement. Both post-impregnation treatments can also decrease the metal-support interaction resulting in increased activity for CO₂ hydrogenation under methanation. Furthermore, addition of ceria was found to increase cobalt reducibility and decrease the metal-support interaction. This led to improve the catalytic performance. By the way, the combination of ceria addition with the post-impregnation treatment did not serve the best catalytic performance. Either ceria promotion or the post-impregnation treatment is indeed.

Department : Chemical Engineering.. Student's Signature

Field of Study : Chemical Engineering Advisor's Signature

Academic Year : 2013

ACKNOWLEDGEMENTS

The authors gratefully thank Office of the Higher Education Commission (CHE) and Higher Education Promotion, and National Research University Development of Chulalongkorn University (CU56-AM10) for the financial support of this project.

CONTENTS

	Page
ABSTRACT IN THAI	iv
ABSTRACT IN ENGLISH.....	v
ACKNOWLEDGEMENTS	vi
LIST OF TABLES	ix
LIST OF FIGURES	xi
CHAPTER	
I. INTRODUCTION	1
II. THEORY AND LITERATURE REVIEWS	1
2.1 Silica porous materials	1
2.2 Ordered SBA materials	5
2.3 Catalyst treatment	10
2.4 Cobalt	10
2.5 Cerium oxide	11
2.6 CO ₂ hydrogenation reaction.....	12
III. EXPERIMENTAL	15
3.1 Catalyst preparation	15
3.2 Catalyst Characterization	20
3.3 Catalyst test in CO ₂ hydrogenation	21
3.4 Research Methodology	26
IV. RESULTS AND DISCUSSION	27
4.1 The effect of post-impregnation treatment on SBA-15 and SBA-16 supported cobalt catalysts.....	27
4.2 The promoting effects of ceria on Co/SBA-15 catalysts	41
4.3 The promoting effects of ceria on Co/SBA-16 catalysts	51
V. CONCLUSIONS AND RECOMMENDATION.....	60
5.1 Conclusions.....	60
5.2 Recommendations.....	61
REFERENCES	62
APPENDICES	67

	Page
APPENDIX A.....	68
APPENDIX B.....	70
APPENDIX C.....	89
APPENDIX D.....	93
VITAE	94

LIST OF TABLES

Table		Page
2.1	Physical properties of mesoporous silicas	5
2.2	Ordered mesoporous silicas prepared by various surfactants	6
2.3	The properties of SBA-15 and SBA-16	9
2.4	Temperature reduction of silica supported cobalt catalyst	11
3.1	The catalyst nomenclature	19
3.2	Operating condition of gas chromatograph	24
4.1	N ₂ physisorption results of SBA-15 and SBA-16	28
4.2	Cobalt oxides distribution results from EDX analysis and their crystallite size	33
4.3	CO ₂ hydrogenation results for Co/SBA-15 and Co/SBA-16 catalysts	40
4.4	Cobalt oxides distribution and their crystallite size of CeO ₂ -promoted Co/SBA-15 catalysts	43
4.5	The catalytic activity of ceria promoted Co/SBA-15 catalysts	50
4.6	The cobalt distribution and the Co ₃ O ₄ crystallite size of CeO ₂ -promoted Co/SBA-16 catalysts	52
4.7	The catalytic activity of ceria promoted Co/SBA-16 catalysts	58
4.8	The comparison of the catalytic performance	59

LIST OF FIGURES

Figure	Page
1.1 CO ₂ emissions from fossil fuel use and cement production per region	1
2.1 Examples of mesoporous structure (a) L α fluid lamellar phase (b) cubic phase (Pm3m) (c) cubic phase (Ia3d) in rod-like representation (d) hexagonal structure	8
2.2 Cerium oxide structure	12
3.1 Flow diagram of CO ₂ hydrogenation system	22
4.1 SAXRD patterns of SBA-15 and SBA-16	29
4.2 XRD patterns of Co/SBA-15 and Co/SBA-16 catalysts	29
4.3 TEM images of SBA-15 and SBA-16 supports	31
4.4 TEM images of different catalyst samples	31
4.5 SEM images (a) SBA-15 (b) SBA-16	32
4.6 TPR profiles of different post-impregnation treatments of Co/SBA-15 and Co/SBA-16 catalysts	36
4.7 XRD patterns of Co/SBA-16-N catalyst (a) before reduction (b) after reduction	37
4.8 XRD patterns of ceria promoted Co/SBA-15 catalysts prepared by (a) co-impregnation (b) sequential impregnation	45
4.9 TPR patterns of Co/SBA-15 and ceria promoted Co/SBA-15 catalysts with post-impregnation treatment	48
4.10 XRD patterns of ceria promoted Co/SBA-16 catalysts prepared by (a) co-impregnation (b) sequential impregnation	53

LIST OF FIGURES

Figure	Page
4.11 TPR patterns of Co/SBA-16 and ceria promoted Co/SBA-16 catalysts with post-impregnation treatment	56
A.1 The SEM/EDX result of Co/SBA-15-N	71
A.2 The SEM/EDX result of Co/SBA-15-U	72
A.3 The SEM/EDX result of Co/SBA-15-V	73
A.4 The SEM/EDX result of Co/SBA-16-N	74
A.5 The SEM/EDX result of Co/SBA-16-U	75
A.6 The SEM/EDX result of Co/SBA-16-V	76
A.7 The SEM/EDX result of Co-Ce/SBA-15-N	77
A.8 The SEM/EDX result of Co/Ce-SBA-15-N	78
A.9 The SEM/EDX result of Co-Ce/SBA-15-U	79
A.10 The SEM/EDX result of Co/Ce-SBA-15- U	80
A.11 The SEM/EDX result of Co-Ce/SBA-15- V	81
A.12 The SEM/EDX result of Co/Ce-SBA-15- V	82
A.13 The SEM/EDX result of Co-Ce/SBA-16- N	83
A.14 The SEM/EDX result of Co/Ce-SBA-16- N	84
A.15 The SEM/EDX result of Co-Ce/SBA-16- U	85
A.16 The SEM/EDX result of Co/Ce-SBA-16- U	86
A.17 The SEM/EDX result of Co-Ce/SBA-16- V	87

A.18 The SEM/EDX result of Co/Ce-SBA-16- V	88
A.19 The area under the peak of CO ₂	90
A.20 The area under the peak of CH ₄	91
A.21 The calibration curve for CO ₂	92
A.22 The calibration curve for CH ₄	92

CHAPTER I

INTRODUCTION

In 2010, the environmental statistics show that total amount of CO₂ emissions are 33 billion tons, and increases every year, which 30 percent increase from 2000 and 45 percent increase from 1990. The top six emitting countries are responsible for 70 percent of total global emissions and the top 25 emitting countries more than 80 percent of total emissions. From the figure below, CO₂ emissions have constant levels which are the most common in the industrial countries. Then, developing process and material used in industrials should also be done.

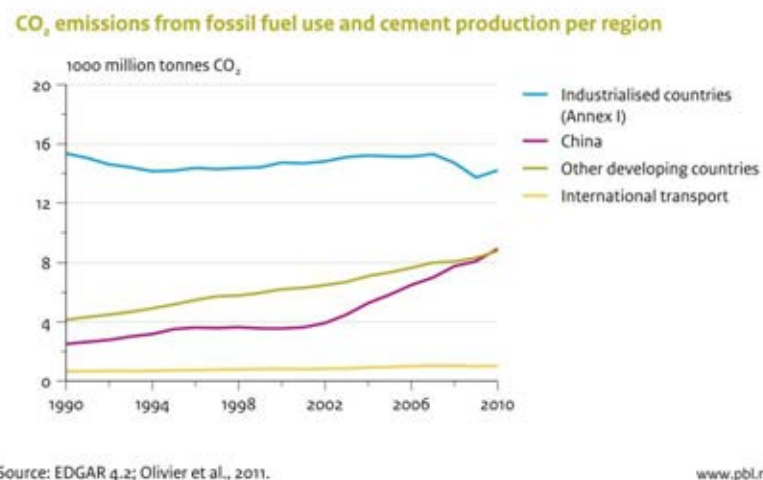


Figure 1 CO₂ emissions from fossil fuel use and cement production per region

CO₂ hydrogenation generates wide range of hydrocarbon elements from carbon dioxide and hydrogen. In the laboratory, the catalysts are used to increase the

chemical reaction rate and conversion. Generally, many transition metal oxides have become interesting catalyst for developing hydrogenation process [1]. Cobalt is the most widely used catalyst because of its high resistance to deactivation, inexpensive and low hazardous. However, cobalt would become low attrition resistance without support. Nowadays, the catalyst is not yet fully developed. There are many ways to create the better catalyst. For example, changing the catalyst precursor can improve the catalytic performance. One of the best ways reported by new researchers of catalysis field is using treatments during impregnation step. The ultrasound treatment and vacuum impregnation are recommended by Pirola *et al.* [2] and Zhao *et al.*[3], consequently. The ultrasound treatment diminishes the crystallize size resulting in improvement of the metal cluster distribution. The vacuum impregnation technique displays small cluster, which states in the pore of support. The small cluster makes vigorous interaction between cobalt and support. Treated catalysts increased productivity. Besides, promoter addition is important to alter the selectivity. it has been discovered that addition of CeO_2 increases C_5^+ selectivity at high temperature [4].

The support is a significant factor to improve the catalytic performance. Silica is generally used as a support due to its good stability under high temperature, controllable morphology and easy to produce. Thus, silica is a good candidate as catalyst support. In recent years, mesoporous silicas, such as SBA-15, SBA-16 and MCM-41, have been developed for several reasons. The mesoporous silica supported cobalt catalysts are the new one for CO_2 hydrogenation. The advantages of

mesoporous silicas are high specific surface area, high pore volume and uniform porous channel structure [5].

This research focuses on the investigation of characteristics and catalytic properties of mesoporous silicas (SBA-15 and SBA-16)-supported cobalt catalysts. In addition, the ultrasound (US) and vacuum treatments were used to improve their catalytic performance. The catalysts were characterized by XRD, TEM, SEM/EDX, N₂ physisorption and TPR. Their catalytic properties were tested in CO₂ hydrogenation under methanation. Moreover, the effect of ceria addition was also investigated. Ceria was added to Co/SBA-15 and Co/SBA-16 catalysts by different preparation methods in order to investigate its effect on metal distribution, reducibility and catalytic performance.

CHAPTER II

THEORY AND LITERATURE REVIEWS

2.1 Silica porous materials

Porous materials are known for many years in medicine [6], composite membrane [7] and other applications [8]. The International Union of Pure and Applied Chemistry (IUPAC) classified porous materials in four groups depending on their pore diameter:

- I. Microporous materials with diameter below 2 nm i.e., zeolite A, X and Y
- II. Mesoporous materials with diameter in range 2-50 nm. For example, FSM-n (Folded Sheet mesoporous Materials-n), MCM 41 (Mobil Composition of Matter No. 41), SBA series, HMS and the others [9, 10].
- III. Macroporous materials with diameter in range 50-7500 nm
- IV. Megaporous materials with diameter rather than 7500 nm

Microporous silica shows strength better than macroporous silica. Their porosity depends on the preparation method, the nature of acid or base catalyst, pH of the solution, the solvent, the temperature, and the relative humidity [11].

Mesoporous silica is synthesized using super molecular groups or blocks. The structure of mesoporous is classified into three groups;

- Hexagonal array i.e., MCM-41, MSU-H and FSM-16.
- Cubic array i.e., SBA-1, SBA-6, and SBA-16 and MCM-48.
- Lamellar array i.e., MSM-50.

Physical properties of some mesoporous silicas are shown in the Table 2.1.

Table 2.1 Physical properties of mesoporous silicas

Silica type	Surfactant used	Pore size (nm)	Wall thickness (nm)	Pore volume (cm ³ /g)	BET surface area ($\times 10^3$, m ² /mol)
MCM-41	CTAB	2.8	1.4	0.62	75.7
MCM-48	CTAB	2.1	1.3	0.63	80.5
SBA-15	P123	8.2	2.8	1.1	46.3
SBA - 16	F127	4.8	1.1	0.34	49.6

2.2 Ordered SBA materials

SBA is the acronym for Santa Barbara Amorphous for example SBA-1 [12], SBA-3 [13], SBA-15 [10] and SBA-16 [14]. Each number corresponds to the pore structure and surfactant used. The first SBA materials were reported in 1998 by Zhao group [5]. These SBA materials present high surface area and specific pore size in the range of 2-20 nm. Moreover, the existence of mesoporous silica is a benefit for the mass transfer limitation and the concentration of active sites [9]. Ordered mesoporous silica is synthesized by different surfactants. Davidson [15] reported that silica

precursor and the surfactant-template directly affected the mesoporous structure. It can be lamellar, hexagonal, cubic or disordered structure. Table 2.2 shows ordered mesoporous silicas template prepared by various surfactants.

Table 2.2 Ordered mesoporous silicas prepared by various surfactants

	Symbol	Signification	Symmetry
Ordered mesoporous silicas template by cationic surfactants	MCM-50	Mobil Composition of Matter	$L \alpha$
	MCM-41	41: 2D hexagonal	P6mm
	MCM-48	48: cubic	Ia3d
Ordered mesoporous silicas template by neutral copolymers (triblock copolymers)	SBA-15	University of California at Santa Barbara 15: 2-D hexagonal	P6mm
	SBA-12	12: 3D hexagonal	$P6_3/mmc$
	SBA-16	16: cubic	Ia3d
	SBA-11	11: cubic	Pm3m
	SBA-1	1: cage-type, cubic	Pm3n
Disordered mesoporous silicas	KIT-1	Korea advanced Institute of Science and Technology 1: disordered material	
	MSU-X	Michigan State University	

2.2.1 SBA-15

SBA-15 is one of most studies as catalyst support and separation because of its uniform pore size, hexagonal array of one-dimensional cylindrical channels, large surface areas, and high thermal stability [16]. Amphiphilic block copolymer has been used to synthesize SBA-15 as organic structure agents. Poly (ethylene oxide)–poly (propylene oxide)–poly(ethylene oxide) or $\text{PEO}_n\text{-PPO}_M\text{-PEO}_n$ is normally used because of its mesostructure properties, inexpensive and biodegradability.

A hierarchical procedure for synthesizing SBA-15 is mixed the strong acid with triblock copolymer as homogeneous solution. A chemical reaction is started when the silica source, such as tetraethoxysilane (TEOS), tetramethoxysilane (TMOS), and tetrapropoxysilane (TPOS), are mixed with the solution. Heating as-synthesized SBA-15 and calcination in air are needed. The diameter and the wall thickness are under the influence of triblock copolymer used. The PEO block copolymer displays hydrophilicity, while the PPO displays hydrophobicity. The interaction between hydrophobic and hydrophilic is used to control its pore dimension and periodicity [17]. Other factor that directly influences the structure is temperature and concentration. The mesostructure can be formed by aggregation of a liquid crystal in aqueous solution, relies on the temperature and concentration (pH). Changing the conditions, the structure is changed. The structure can be in the form of spherical, cylindrical, lamellar (cubic phase) or disordered (the figure is shown below). A slow condensation rate is an important factor. The formation of mesostructure needs slowly silica condensation rate. The condensation rate increases, as pH is increased. The

smaller size required a longer growth time. From the past research, they found that the slowest growth rate occurred at pH 2-4 [18].

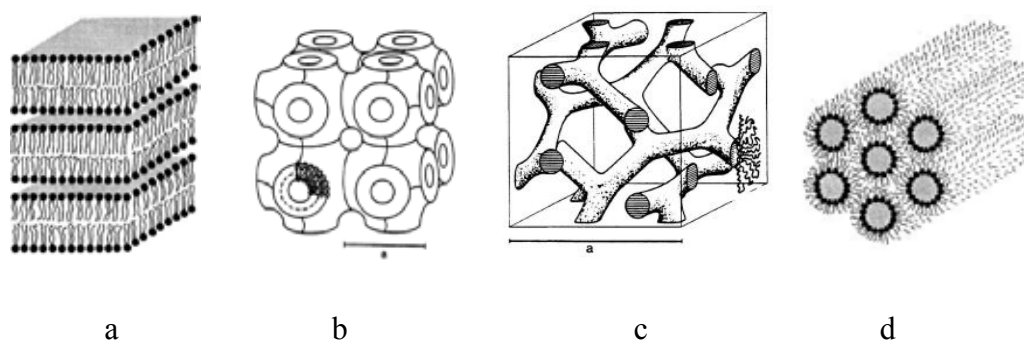


Figure 2.1 Examples of mesoporous structure (a) $L\alpha$ fluid lamellar phase (b) cubic phase (Pm3m) (c) cubic phase (Ia3d) in rod-like representation (d) hexagonal structure

The pore size is also adjusted by addition of trimethylbenzene or TMB. The addition of TMB as a swelling agent leads to increase the pore diameter of SBA-15 [19]. Also, the pore size may be conformed in many ways. The first way is to alter the TMB/block copolymer weight ratio. The pore size can increase with increasing weight ratio. Changing the catalyst precursor is usually used to increase the pore size. For example, many cobalt precursors have been used in Fischer-Tropsch process to study the effect of different precursor. It has been reported that the cobalt acetylacetonate and cobalt acetate precursors confined the cluster inside the pores [20]. Moreover, Ding *et al.* [21] reported that the addition of sodium silicate can control its dimension. Upon to synthesis, quartz and sodium carbonate were mixed with different molar ratios. When the molar ratio increased, the pore wall thickness are increased because of the faster condensation of polysilicate anions. Lu *et al.* [22]

reported about synthesizing SBA-15 without the calcination process. SBA-15 excluding calcination process had high hydrothermal stability because the EO blocks hindered the hydrolysis of Si-O-Si. Interestingly, they also used sulphuric acid instead of HCl acid resulting in removal efficiency of the P123 template.

2.2.2 SBA-16

SBA-16 exhibits a large cage-like pores formed in a three dimensional cubic body-centered Im3m symmetry [23]. The SBA-16 material is prepared under acid condition using non-ionic pluronic as a surfactant template [24]. The morphology control of SBA-16 can be achieved by adjustment of synthesis substances such as solvents, surfactants or salt additions [25]. The preparation of SBA-16 is same as SBA-15, but different surfactant is used. The properties of SBA-15 and SBA-16 are shown in Table 2.3

Table 2.3 The properties of SBA-15 and SBA-16

Application	SBA-15	SBA-16
Surfactant	Pluronic P123	Pluronic F127
Structure	Hexagonal (p6mm symmetry)	cubic body-centered (Im3m symmetry)
Specific surface area	798 m ² /g	447 m ² /g
Pore size	8.2 nm	4.8 nm
Pore volume	1.1 cm ³ /g	0.34 cm ³ /g
Wall thickness	2.8 nm	1.1 nm

2.3 Catalyst treatment

2.3.1 Ultrasound treatment

The traditional impregnation catalysts show low metal dispersion. Therefore, many researchers have worked on making high metal distribution catalysts. Pirola *et al.* [2] reported the advantages of using the ultrasound treatment after impregnation. They indicated that the ultrasound treatment diminishes the crystallize size resulting in improvement of the metal cluster distribution on the support. As this treatment also enhances the catalytic performance compared with the basic impregnation method.

2.3.2 Vacuum impregnation

Another way to make high metal dispersion reported by Zhou *et al.* [26] is the vacuum impregnation. They studied the effect of different environments on the preparation of Co/SiO₂ catalysts, which were impregnated under common and vacuum conditions. The catalyst impregnated under vacuum condition, displays a small cluster, which states in the pore of support making vigorous interaction between cobalt and support. Although the smaller particles show high metal dispersion, the strong interaction also occurs resulting in a decrease of catalytic activity.

2.4 Cobalt

The most common material used in catalysis reaction is cobalt because of various valence states, inexpensive and high resistance to deactivation. Oxide supported cobalt catalysts are more attrition resistant than unsupported cobalt catalyst

[27]. CO₂ hydrogenation generally used cobalt as a catalyst due to its high activities and low pressure operation required [28]. The active cobalt catalyst is in the form of cobalt metallic phase. Then, the reduction process is required. The reduction of Co₃O₄ is a two-step process which passes through an intermediate CoO phase before reduction to the cobalt metal [29]. A weak cobalt support interaction serves high cobalt reducibility. A solid-state reaction between silica and cobalt oxides could also result in mixed oxide, which should be avoided. Minimization of the concentration of cobalt silicate and cobalt metal dispersion would result in a better catalytic performance [30]. Temperature reduction of silica supported cobalt catalyst has been shown below [31].

Table 2.4 Temperature reduction of silica supported cobalt catalyst

Cobalt phase	Temperature reduction
Co ₃ O ₄ →CoO	145-230 °C
CoO→Co ⁰	255-335 °C
CoSiO ₄	> 550 °C

2.5 Cerium oxide

Cerium oxide is commonly used in the form of promoter for supported catalysts because of its enhancement:

- To stabilize the metal cluster dispersion on the support
- To improve the oxidation and reduction of the metal
- To enhance oxygen storage and free by shifting between CeO₂ under reducing condition

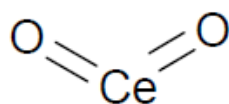


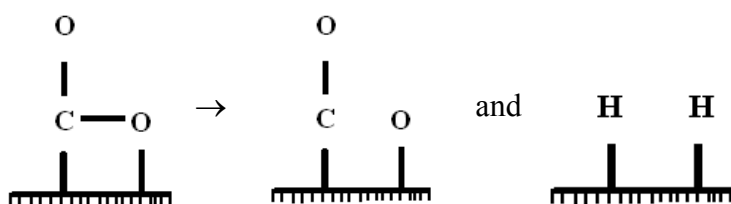
Figure 2.2 Cerium oxide structure

There are many reports about ceria promoted catalysts. Dorner *et al.* [32] studied in the effect of ceria promoted Fe/Mn/K catalysts. They found that ceria promoted catalyst exhibited an increase activity and selectivity in CO₂ hydrogenation reaction.

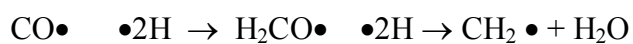
2.6 CO₂ hydrogenation reaction

CO₂ hydrogenation reaction has CO₂ as a reactant, which can produce various hydrocarbon products. So, this reaction has aroused increasing interest for solving the environmental problem. Cobalt, iron, ruthenium and nickel are good candidates, but other group VIII metals can also be used. As expected, cobalt and nickel are widely used as a catalyst [33]. Interestingly, cobalt catalyst exhibit higher CO₂ hydrogenation activity than nickel catalyst [34]. Furthermore, the lower operating temperature is preferred for cobalt catalysts [35]. Previous researches revealed many possible reaction pathway of CO₂ hydrogenation. Zhao *et al.* [36] said these are five steps, Reactant adsorption, chain initiation, chain growth, chain termination and the product desorption.

Reactant adsorption occurs at the catalyst surface;

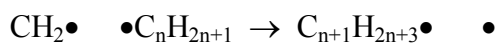


chain initiation;

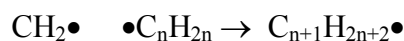


When $\text{CH}_2\bullet$ is intermediate form to continue chain insertion and \bullet is shown as active site.

chain growth with metal-alkyl bond insertion;

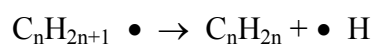


Or with metal-alkylidene insertion;

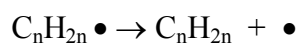


Last, chain termination occurs when hydrogen in β -site is eliminated.

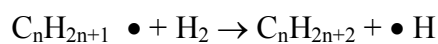
The formation of alkene products;



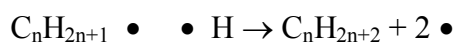
Or



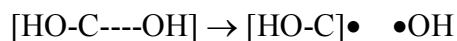
The formation of alkane products;



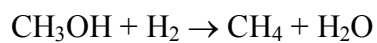
Or



Zhang *et al.* [37] reported CO₂ hydrogenation mechanism that the bond breaking occurs at C-O bonds, which is called dissociative of CO₂ molecule. The H molecule is added to both sides. The OH group is removed from the reaction as water.



Second, the hydrogenation of intermediate performs the intermediate methanol, adding the H molecule to form the hydrocarbon products [Y.Zhang, 2002 #59].



CHAPTER III

EXPERIMENTAL

This section consists of three parts: (i) catalyst preparation, (ii) catalyst characterization and (iii) procedure for CO₂ hydrogenation process. Catalyst preparation section describes the chemical used to prepare cerium promoted and unpromoted cobalt catalysts. Catalyst characterization section describes the techniques used for characterizing catalysts include: X-ray diffractomete (XRD), Temperature-programmed reduction (TPR), N₂ physisorption (BET), transmission electron microscopy (TEM) and CO chemisorption. The last session is to understand the CO₂ hydrogenation process.

3.1 Catalyst preparation

3.1.1 Chemicals

Chemicals used in this experiment are shown below.

- 1) Pluronic acid P123 imported form Sigma-Aldrich Co. Lcc.
- 2) Pluronic acid F127 imported form Sigma-Aldrich Co. Lcc.
- 3) Hydrochloric acid 37% imported form QREC
- 4) Tetraethyl orthosilicate 98% (TEOS) imported form Sigma-Aldrich Co. Lcc.
- 5) Cobalt (II) nitrate hexahydrate $\geq 98\%$ imported form Sigma-Aldrich Co. Lcc.
- 6) Cerium (III) nitrate hexahydrate 99.9% imported form Sigma-Aldrich Co. Lcc.

3.1.2 Preparation of support

Two types of mesoporous silicas, SBA-15 and SBA-16, were synthesized based on the procedure described by Zhao *et al.* [17], as follows:

- SBA-15

For SBA-15 synthesis, 4 g of pluronic P123 was added into the solution of 120 g of 2M HCl acid and 30 g of deionized water. After stirring, a clear solution was obtained. Then, 8.5 g of TEOS was added into the solution. The mixture was stirred for 20 h at room temperature followed by aging at 80 °C for 24 h. The template was removed by washing with deionized water for 5-7 times followed by filtration. Then, the mixture was dried at room temperature and calcined in air at 500 °C for 6 h with heating rate of 10 °C/min.

- SBA-16

The synthesis procedure of SBA-16 was similar to that of SBA-15, but using pluronic F127 as a template. 1.5 g of pluronic F127 was added into the solution of 120 g of 2M HCl and 30 g of deionized water. 8.5 g of TEOS was added to the clear mixture and stirred for 20 h at room temperature followed by aging at 105 °C for 48 h. The resulting solid was obtained by washing with DI water and filtering. The solid particles were dried at room temperature followed by calcination at 560 °C for 4 h with heating rate of 1 °C/min.

3.1.3 Preparation of catalyst

The cobalt catalysts were prepared by using cobalt (II) nitrate hexahydrate [Co(NO₃)₂•6H₂O] as a precursor with 20 wt% of cobalt loading on the SBA-15 and

SBA-16 supports. DI water was used to dissolve the catalyst precursor. Then, the cobalt solution was dropped into the support by incipient wetness impregnation. Catalysts were denoted as Co/SBA-15-N and Co/SBA-16-N.

- **Post-impregnation treatment**

There were two post-impregnation treatment methods having details as follows;

(i) Ultrasound treatment was used after impregnation, as mentioned above. After the impregnation step, a porcelain consisting of the catalyst, was placed into a sonicator. The catalyst was sonicated for 30 min at room temperature. Catalyst was named as Co/SBA-15-U or Co/SBA-16-U.

(ii) Vacuum impregnation is another way to increase the metal dispersion. It was performed after the impregnation step. The wet catalyst was transferred into filtration flask. Then, a vacuum condition was created in the flask by removing air from the flask using a vacuum pump at room temperature for 30 min. The catalyst was named as Co/SBA-15-V and Co/SBA-16-V.

Then, all catalysts were dried at 105 °C for 12 h and calcined in air at 500 °C for 6 h.

3.1.4 Preparation of the modified-silica supported

A modified-silica support was prepared by incipient wetness impregnation. A cerium (III) nitrate hexahydrate (5 wt% loading) was dissolved in the water. Then, the solution was slowly dropped to the support. The modified-support was dried at room temperature and calcined in air at 450 °C for 3 h with heating rate of 10 °C/min.

3.1.5 Preparation of ceria promoted cobalt catalyst

- Co-impregnation method

The prepared supports from 3.1.2 were impregnated with an aqueous solution of 20% Cobalt (II) nitrate hexahydrate and 5% cerium (III) nitrate hexahydrate. The materials obtained are treated by ultrasound treatment and vacuum impregnation. The catalysts are denoted as Co-Ce/SBA-15-N, Co-Ce/SBA-15-U, Co-Ce/SBA-15-V, Co-Ce/SBA-16-N, Co-Ce/SBA-16-U and Co-Ce/SBA-16-V.

- Sequential impregnation method

The modified supports from 3.1.3 were impregnated with an aqueous solution of 20% Cobalt (II) nitrate hexahydrate. Ultrasound treatment and vacuum impregnation was used after impregnation process. The catalysts was named as Co/Ce-SBA-15-N, Co/Ce-SBA-15-U, Co/Ce-SBA-15-V, Co/Ce-SBA-16-N, Co/Ce-SBA-16-U and Co/Ce-SBA-16-V.

The catalysts will be dried at room temperature and calcined in air at 500 °C for 4 h with heating rate 10 °C/min.

The catalyst nomenclature is shown in Table 3.1

Table 3.1 The catalyst nomenclature

Catalyst name	Support		Ceria modified method	Post-impregnation method
	SBA-15	SBA-16		
Co/SBA-15-N	○		×	Non
Co/SBA-15-U	○		×	US treatment
Co/SBA-15-V	○		×	Vacuum
Co/SBA-16-I		○	×	Non
Co/SBA-16-U		○	×	US treatment
Co/SBA-16-V		○	×	Vacuum
Co/Ce-SBA-15-N	○		Sequential	Non
Co/Ce-SBA-15-U	○		Sequential	US treatment
Co/Ce-SBA-15-V	○		Sequential	vacuum
Co-Ce/SBA-15-N	○		Co-impregnation	Non
Co-Ce /SBA-15-U	○		Co-impregnation	US treatment
Co-Ce /SBA-15-V	○		Co-impregnation	Vacuum
Co/Ce-SBA-16-N		○	Sequential	Non
Co/Ce-SBA-16-U		○	Sequential	US treatment
Co/Ce-SBA-16-V		○	Sequential	Vacuum
Co-Ce /SBA-16-N		○	Co-impregnation	Non
Co-Ce /SBA-16-U		○	Co-impregnation	US treatment
Co-Ce /SBA-16-V		○	Co-impregnation	Vacuum

3.2 Catalyst Characterization

3.2.1 Small angle X-ray diffraction (SAXRD)

Small angle X-ray diffraction (SAXRD) is a technique used to identify the chemical structure of the support. The Bruker AXS Model D8 Discover X-ray diffractometer having a VÅNTEC-1 detector (Super Speed Detector) connected to computer was used. It was carried out by using Cu radiation that was scanned at a rate of 0.3 second/step in the 2θ range of 0.5-6 degrees resolution of 0.02°.

3.2.2 X-Ray Diffraction (XRD)

The SIEMENS D-5000 X-ray diffractometer connected to a computer with Diffract ZT version 3.3 program was used for the XRD measurement of the catalysts. The experiment was carried out by using K_{α} ($\alpha=1.54439 \text{ \AA}$) radiation with Ni filter. The spectra were scanned at a rate of 0.02 degree/min in the 2θ of 15-80 degrees with a resolution of 0.04°.

3.2.3 Temperature programmed reduction (TPR)

Temperature programmed reduction (TPR) measurements at 35-800°C were performed on a Micrometric Pulse Chemisorb 2750 instrument. 0.05 g of catalyst samples was pretreated in 15 ml/min of helium flowing at 100°C for 1 h with a heating rate of 10 °C/min. After cooling down to room temperature, a flow of H₂/Ar (15 ml/min) was passed through the samples while the temperature was raised to 800 °C with heating rate of 1 °C/min.

3.2.4 N₂ physisorption

The nitrogen physisorption was performed for determining the specific surface area, pore size and pore volume of the supports, using Micromeritics ASAP 2020 equipment at -196 °C. Before the measurement step, SBA-15 and SBA-16 were outgases at 200 °C and at 250 °C for 3 h, consequently.

3.2.5 Transmission electron microscopy (TEM)

Transmission electron microscopy will be used to determine the morphologies of catalyst and cobalt particle size using JEOL JEM-2101.

3.2.6 Scanning electron microscope/energy dispersive X-ray spectroscopy (SEM/EDX)

The morphology of the catalysts was determined by scanning electron microscopy (SEM) using JEOL mode JSM-6400. Consequently, EDX measures the elemental distribution in catalysts using Link Isis series 300 program.

3.3 Catalyst test in CO₂ hydrogenation

3.3.1 Apparatus

Flow diagram of CO₂ hydrogenation catalyst testing is shown in Figure 3.1 which consists of reactor, an automatic temperature controller, furnace, gas chromatography and gas controlling system.

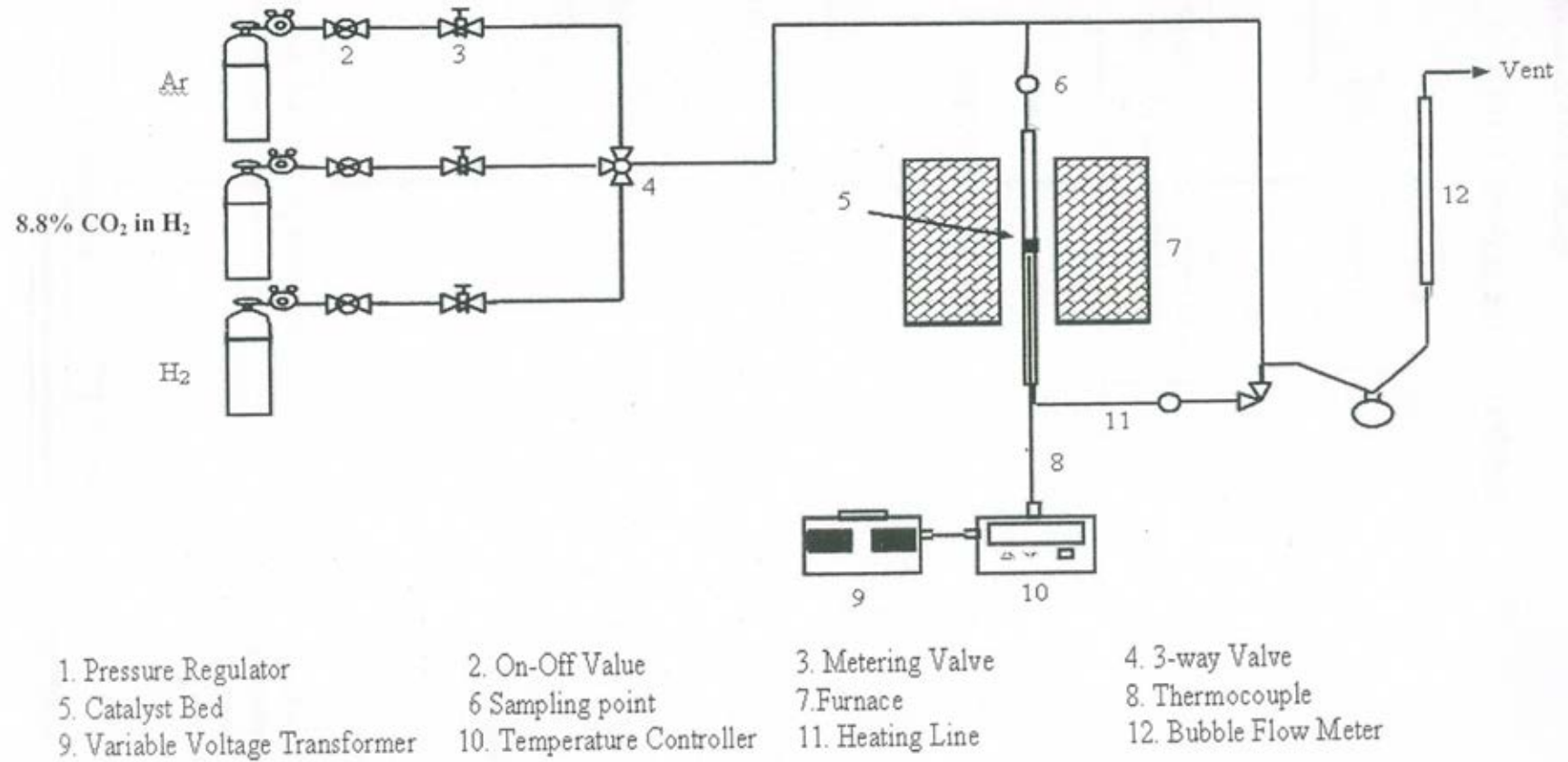


Figure 3.1 Flow diagram of CO₂ hydrogenation system

3.3.1.1 Reactor

The reactor made from the stainless steel tube, which has outer diameter 3/8 inch. The products were collected above and below the catalyst bed. The catalyst was placed into the reactor above quartz wool.

3.3.1.2 Automatic Temperature Controller

This unit consisted of a magnetic switch connected to a variable voltage transformer and a solid-state relay temperature controller model no. SS2425DZ connected to a thermocouple. Reactor temperature was measured at the bottom of the catalyst bed in the reactor. The temperature control set point is adjustable within the range of 0-800 °C at the maximum voltage output of 220 volt.

3.3.1.3 Electrical Furnace

The furnace supplied heat to the reactor for CO₂ hydrogenation. The reactor could be operated from temperature up to 800 °C at the maximum voltage of 220 volt

3.3.1.4 Gas Controlling System

Reactant for the system was each equipped with a pressure regulator and an on-off valve and the gas flow rates were adjusted by using metering valves.

3.3.1.5 Gas Chromatography

The composition of hydrocarbons in the product steam was analyzed by a Shimadzu GC14B (VZ10) gas chromatograph equipped with a flame ionization detector. A Shimadzu GC8A (molecular sieve 5A⁰ and Porapak Q) gas chromatography equipped with a thermal conductivity detector was used to analyze CO₂, CO and H₂ in the feed and product steams. The operating conditions for each instrument are shown in the Table 3.2.

Table 3.2 Operating condition of gas chromatograph

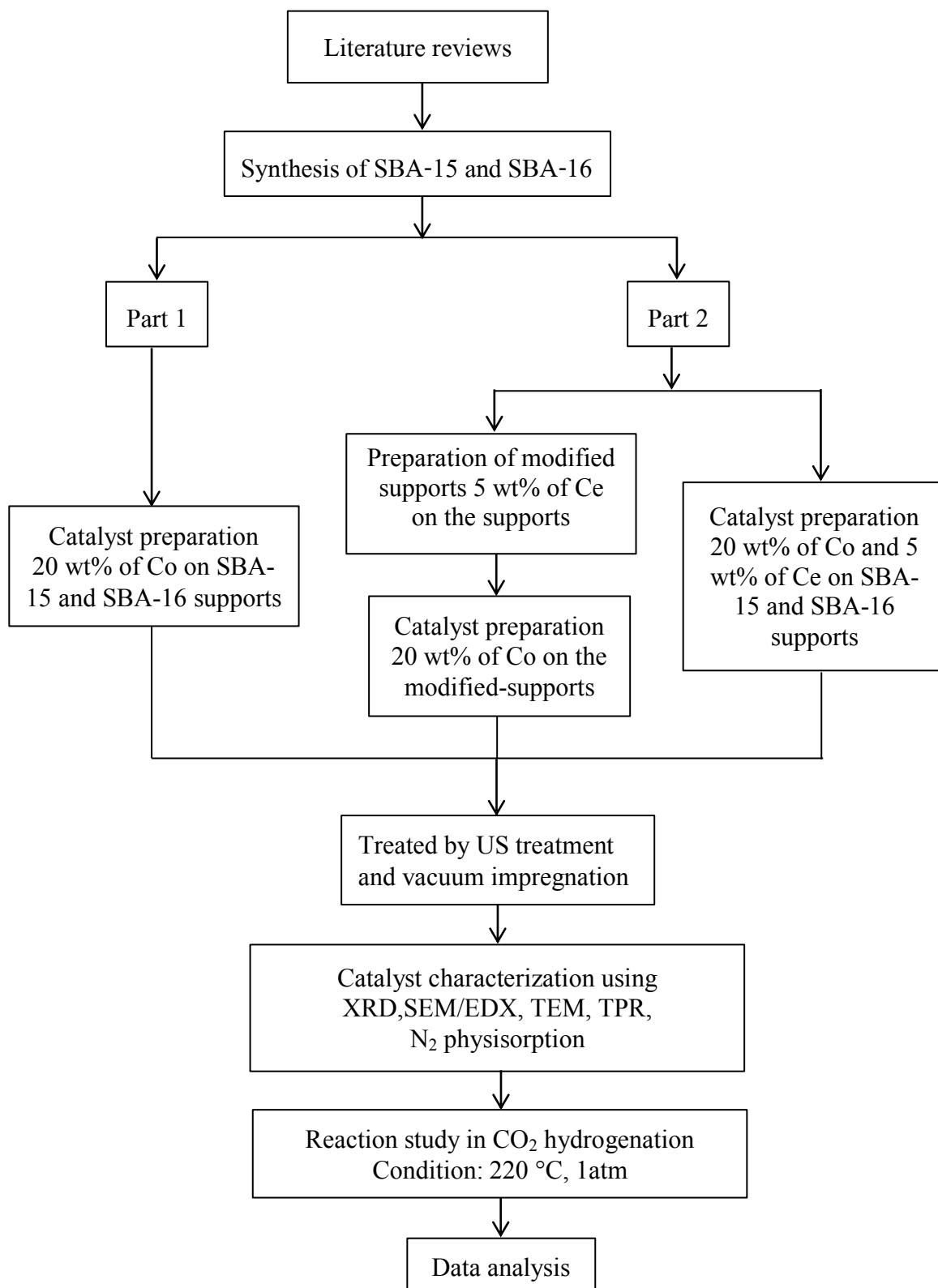
Gas chromatograph	SHIMADZU GC-8A	SHIMADZU GC-14B
Detector	TCD	FID
Column	Porapak Q molecular sieve 5A ⁰	VZ 10
-Column material	SUS	-
-Length	2m	-
-Outer diameter	4mm	-
-Inner diameter	3mm	-
-Mesh range	60/80	60/80
-Maximum temperature	623 K	353 K
Carried gas	He (99.999%)	H ₂ (99.999%)
Carried gas flow	40 cc/min	-
Column gas	He (99.999%)	Air , H ₂
Column gas flow	40 cc/min	-
Column temperature		

-initial (°C)	60	70
-final (°C)	60	70
Injector temperature (°C)	100	100
Detector temperature (°C)	100	150
Current (mA)	80	-
Analysed gas	Ar, CO, CO ₂ , H ₂	Hydrocarbon C1-C4

3.3.2 Procedures

CO₂ hydrogenation was performed using 3/8" fixed-bed microreactor. 0.1 g of catalysts was packed over the quartz wool. First, the catalyst was pretreated in 50 ml/min of H₂ flowing, while the temperature was raised to 350 °C from room temperature. After the temperature reached 350 °C, the catalyst was held for 3 h. Then, it was cooled down to 220 °C. Then, H₂/CO₂ having the ratios of 10/1 was fed into the reactor at the flow rate of 22.4 ml/min. Products were analyzed by GC. Two columns were used to detect reactant and product gas, consisting of CO, CO₂ and CH₄. The thermal conductivity detector (*TCD*) was used to detect CO and CO₂, while flame ionization detection (*FID*) was used to detect CH₄ and larger hydrocarbons.

3.4 Research Methodology



CHAPTER IV

RESULTS AND DISCUSSION

Aim of this chapter is to describe the result and discussion which are separated into three parts. First, section 4.1 reports the effect of post-impregnation treatment on SBA-15 and SBA-16 supported cobalt catalysts. To examine conversion and activity, the catalysts were tested in the CO₂ hydrogenation reaction. Next, section 4.2 presents the promoting effect of ceria on Co/SBA-15 catalysts with post-impregnation treatments. Section 4.3 explains the promoting effect of ceria on Co/SBA-16 catalysts with post-impregnation treatments.

4.1 The effect of post-impregnation treatment on SBA-15 and SBA-16 supported cobalt catalysts

4.1.1 N₂ physisorption

N₂ physisorption was used to determine the specific surface area of SBA-15 and SBA-16, including pore size and pore volume. The textural properties are summarized in Table 4.1. Both of mesoporous silicas have large surface areas. The SBA-15 has a surface area of 674 m²/g, while the SBA-16 has slightly lower surface area of 664 m²/g. Therefore, the SBA-15 implies more hydrothermal stable.

Table 4.1 N₂ physisorption results of SBA-15 and SBA-16

support	BET surface area (m²/g)	Pore volume (cm³/g)	Pore size (nm)
SBA-15	674	0.66	3.92
SBA-16	664	0.43	2.61

4.1.2 X-ray diffraction (XRD)

The SAXRD patterns (Figure 4.1) at low diffraction angle were essentially confirmed the mesoporous silica structure of SBA-15 and SBA-16. For the SBA-15, the presence of reflection index according to (100), (110) and (200) confirms 2D hexagonal symmetry, which is in agreement with those from Zhao *at al.*[17]. The diffraction peaks of SBA-16 could be indexed in the cubic structure as (100), (111) and (200), respectively [38]. After impregnation process, XRD patterns with wide diffraction angles revealed the crystalline Co₃O₄ species for all catalysts, as shown in Figure 4.2. The diffraction peaks at 2θ≈19, 31.3, 36.9, 44.9, 59.4, 65.3 surely indicate the cobalt oxide species (Co₃O₄) over the supports for all impregnation methods [1].

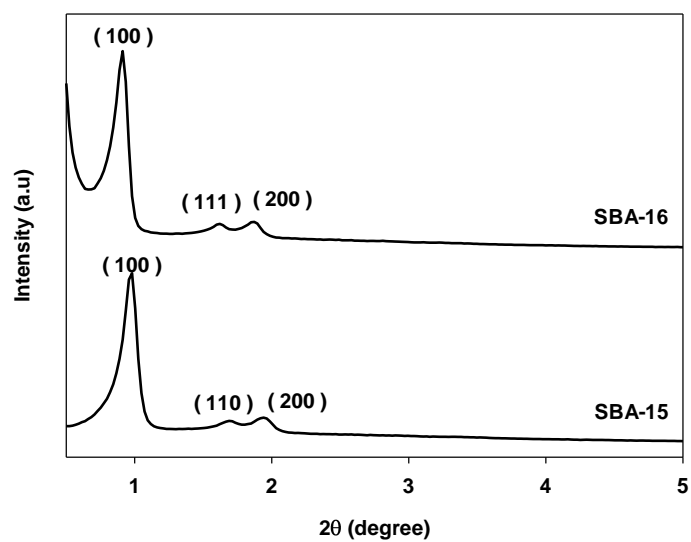


Figure 4.1 SAXRD patterns of SBA-15 and SBA-16

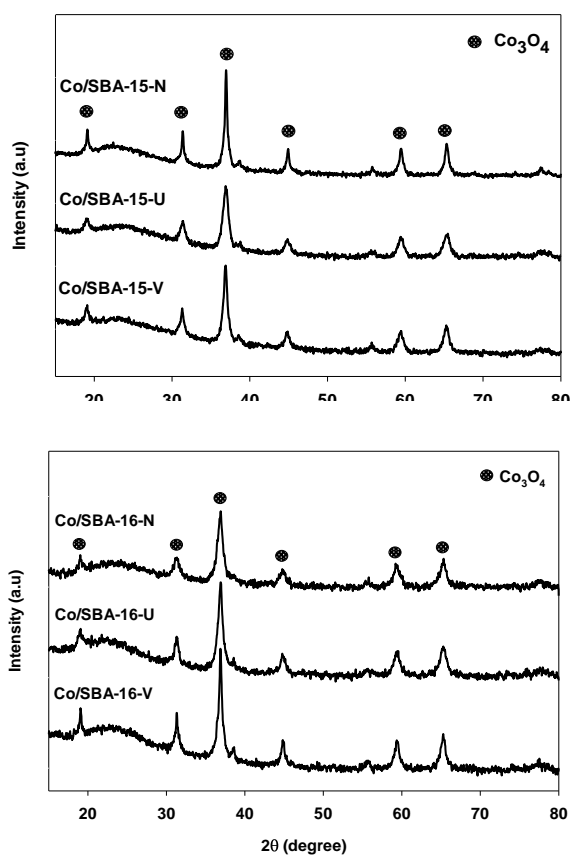


Figure 4.2 XRD patterns of Co/SBA-15 and Co/SBA-16 catalysts

4.1.3 Transmission electron microscopy (TEM)

The TEM images are shown in Figure 4.3, it is an alternative way to identify the structure of SBA-15 and SBA-16. The SBA-15 presents a hexagonal structure like honeycomb. On the other hand, the SBA-16 displays cubic body centered like cage structure connected in worm-like shape. The other TEM images are shown in Figure 4.4 in order to observe cobalt oxide distribution. It is clearly seen that the non-treatment catalysts produced larger cobalt oxide crystallites than the post-impregnation treatment catalysts. The smaller the cobalt oxide crystallites displayed the greater distribution. This is consistent with previous reports [2] that the post-impregnation treatment using US and vacuum impregnation improved the better metal dispersion. Interestingly, the catalysts using vacuum impregnation as a treatment showed that the cobalt oxide crystallites were located in the inner pore, while US treatment produced cobalt oxide crystallites present outer the silica surface.

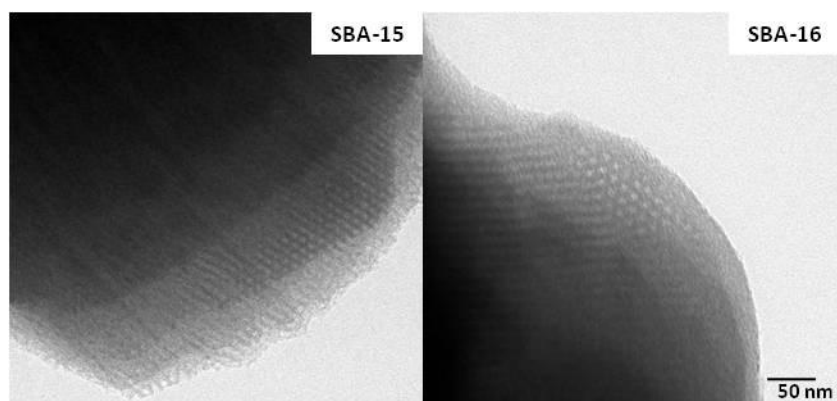


Figure 4.3 TEM images of SBA-15 and SBA-16 supports

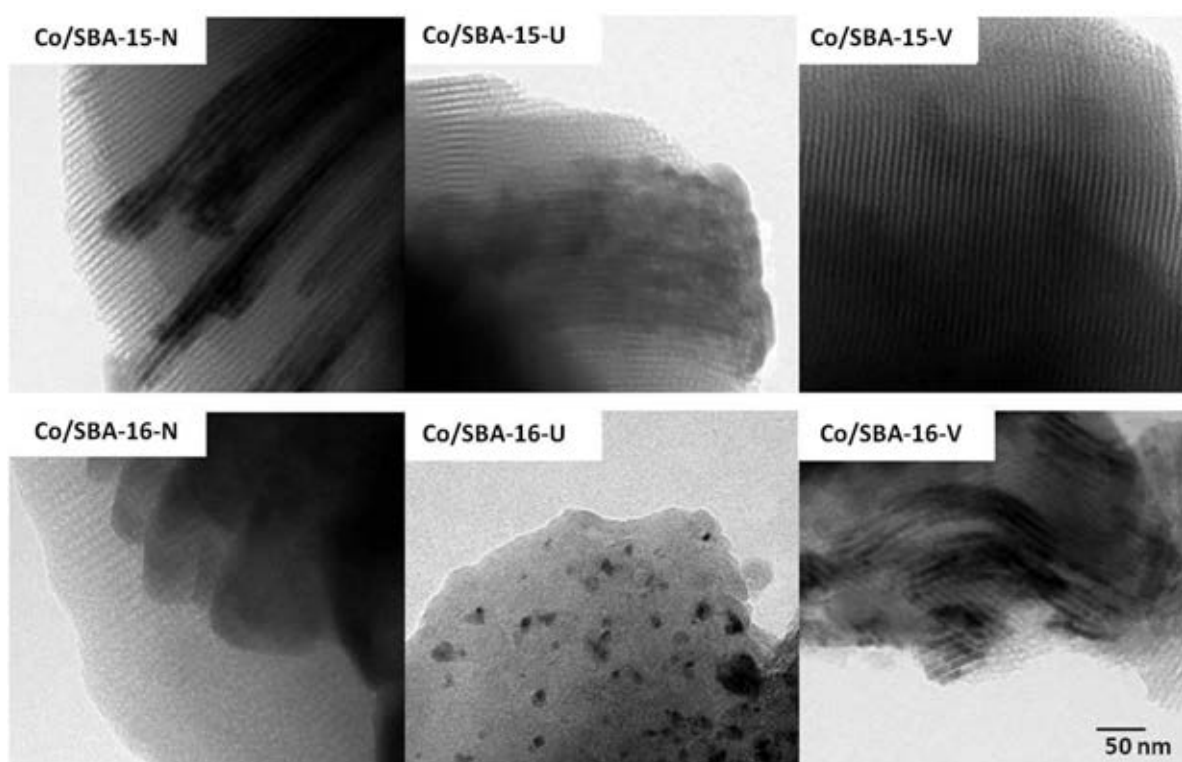


Figure 4.4 TEM images of different catalyst samples

4.1.4 Scanning electron microscopy (SEM) and Energy dispersive X-ray spectroscopy (EDX)

To study the morphology of SBA-15 and SBA-16, SEM was used. Morphologies of SBA-15 and SBA-16 are illustrated in Figure 4.5a and Figure 4.5b, respectively. A collection of the SEM micrographs can be seen below.

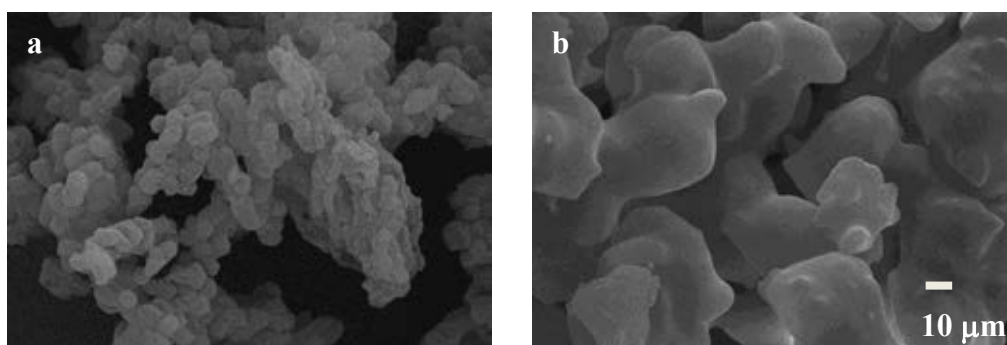


Figure 4.5 SEM images (a) SBA-15 (b) SBA-16

The amounts of cobalt distribution based on the EDX measurement are shown in **Table 4.2** revealing how well cobalt oxides can distribute over the silica near surface. For example, the cobalt distribution of Co/SBA-15-N is 28.18%. This means that based on 100% of sample surface, the cobalt on the surface is 28.18%. From the result, it was found that the post-impregnation treatments increased the metal distribution according to TEM results and those reports [2,3]. The content of cobalt oxide decreased in the order of US treatment > vacuum treatment > none treatment. As far as we know, the metal crystallite size is inversely proportional to distribution. The post-impregnation treatments lead to an increase in metal distribution due to decreasing the metal size [39]. However, this result could not explain the total dispersion properties of the catalysts because dispersion properties are considered

based on the metal form. In fact, different support is a significant factor to raise the metal distribution [40]. Although SBA-15 exhibited better physical properties than SBA-16, SBA-16 served better metal distribution than SBA-15 due to its unique properties.

Table 4.2 Cobalt oxides distribution results from EDX analysis and their crystallite size

sample	wt% Cobalt on support ^a	Cobalt oxide crystallite size (nm) ^b
Co/SBA-15-N	28.18	17.6
Co/SBA-15-U	45.90	20.2
Co/SBA-15-V	38.48	22.6
Co/SBA-16-N	49.16	14.1
Co/SBA-16-U	75.81	19.1
Co/SBA-16-V	49.36	16.0

^a from the EDX analysis

^b from the XRD analysis

4.1.5 Temperature-programmed reduction (TPR)

Temperature programmed reduction (TPR) is one of the most powerful techniques to identify the reduction behaviors of catalysts regarding to the metal dispersion and metal-support interaction. For a better understanding, the reduction behaviors as shown in Figure 4.6 are illustrated as the TPR profiles of different samples. A typical reduction of silica- supported cobalt catalyst is commonly occurred at temperature ranging from 200-600 °C [1,40,41]. The reduction is accomplished in two steps; $\text{Co}^{3+} \rightarrow \text{Co}^{2+}$ appears in temperatures ranging from 220-320°C and $\text{Co}^{2+} \rightarrow \text{Co}^0$ occurs at temperatures in the range of 320-500°C. Cobalt silicate can be formed when the temperature is raised above 500 °C [1] upon the types of support used. Among the SBA-15 supported cobalt catalysts, the Co/SBA-15-N shows two step reduction and strong metal-support interaction, while other catalysts exhibit only a single broad peak due to their uniform small cobalt crystallite size dispersed on the support. From the previous report [42], they reported that there are two types of metal-support interaction; (i) upon the strong metal-support interaction, the small metal particles is more difficult to reduce than large particles, and (ii) upon the weak interaction, the large particles is more difficult to reduce when compared to small particle. As a result, TPR profiles of Co/SBA-15-U and Co/SBA-15-V clearly showed that the post-impregnation treatment can reduce the metal-support interaction and the reduction temperature was shifted to lower temperature. This is because the metal-support interaction of SBA-15 and SBA-16 are weak interaction. Post-impregnation treatments introduced small metal particles, and hence is easily reduced compared to

the large particles. Besides, a single reduction peak was shown in the case of Co/SBA-15-U and Co/SBA-15-V to be due to uniform crystallite size.

Among the SBA-16 supported cobalt catalysts, TPR profile of Co/SBA-16-N shows high metal-support interaction as same as Co/SBA-15-N. When the US treatment was applied to the SBA-16 supported catalysts, the Co/SBA-16-U still displayed high metal-support interaction that contrasts of Co/SBA-15-U. This evidence confirmed that there are other factors affected on the reduction behavior. Hence, the US treatment is only suitable for SBA-15 supported catalysts due to the nature of support. Based on the TPR profiles in Figure 4.6, the vacuum impregnation seems to be the best way to increase the metal distribution and diminish interaction for both of Co/SBA-15 and Co/SBA-16 catalysts based on the TPR results. For better understanding, Scheme 1 is illustrated based on the TPR measurement. In order to determine whether or not cobalt silicate was formed after TPR measurement, the reduced catalyst (Co/SBA-16-N) was characterized with XRD. The XRD patterns obtained from the reduced Co/SBA-16-N catalyst is given in Figure 4.7. Considering the XRD pattern of the calcined Co/SBA-16-N catalyst, it showed only the cobalt oxide species (Co_3O_4) as mentioned before, whereas the XRD patterns of the reduced one presented cobalt metal in the fcc and hcp crystallographic forms [43]. However, no XRD peaks of cobalt silicate were detected or the crystallite size of cobalt silicate was less than 3 nm and being in the highly dispersed form.

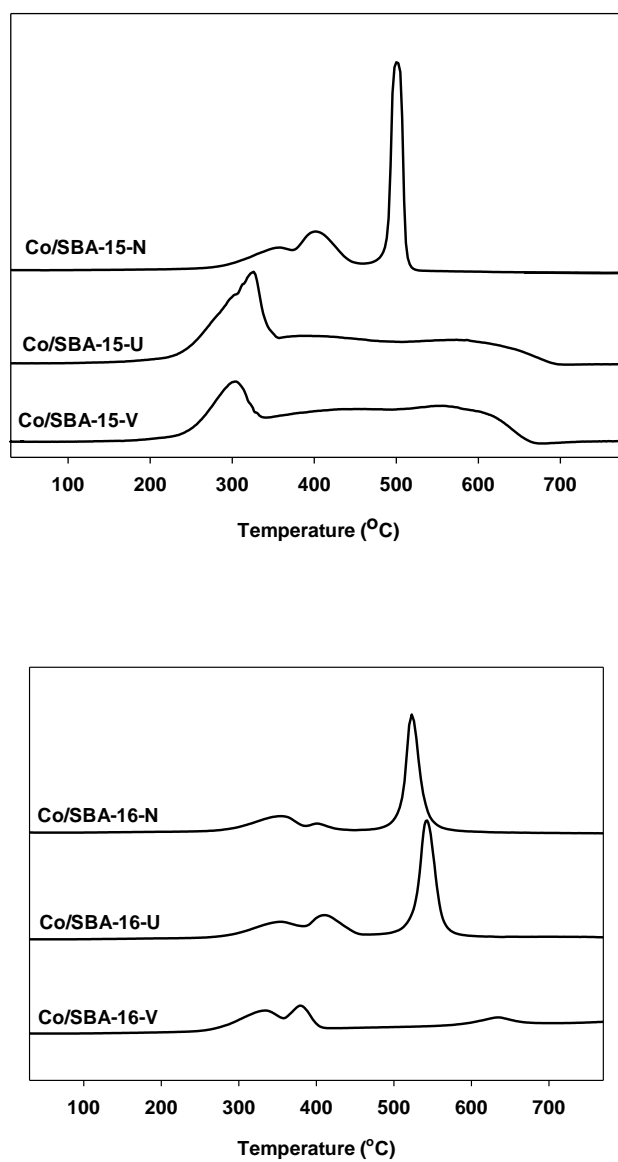


Figure 4.6 TPR profiles of different post-impregnation treatments of Co/SBA-15 and Co/SBA-16 catalysts

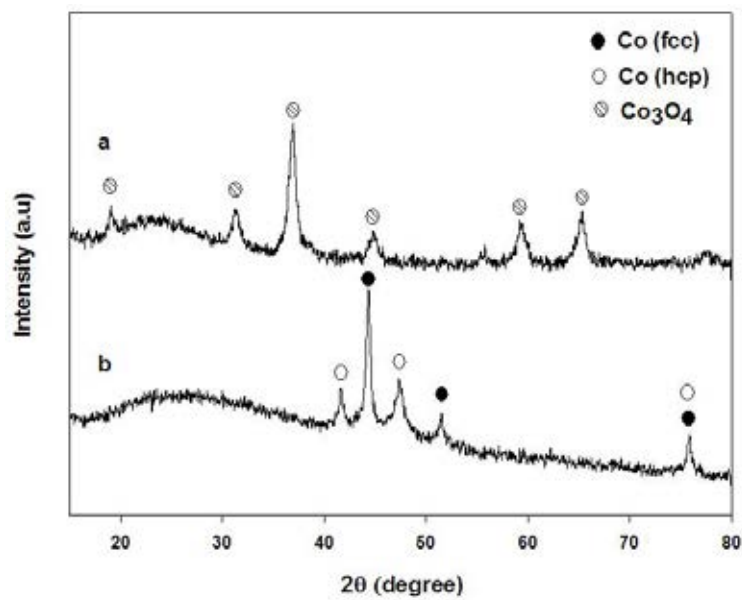
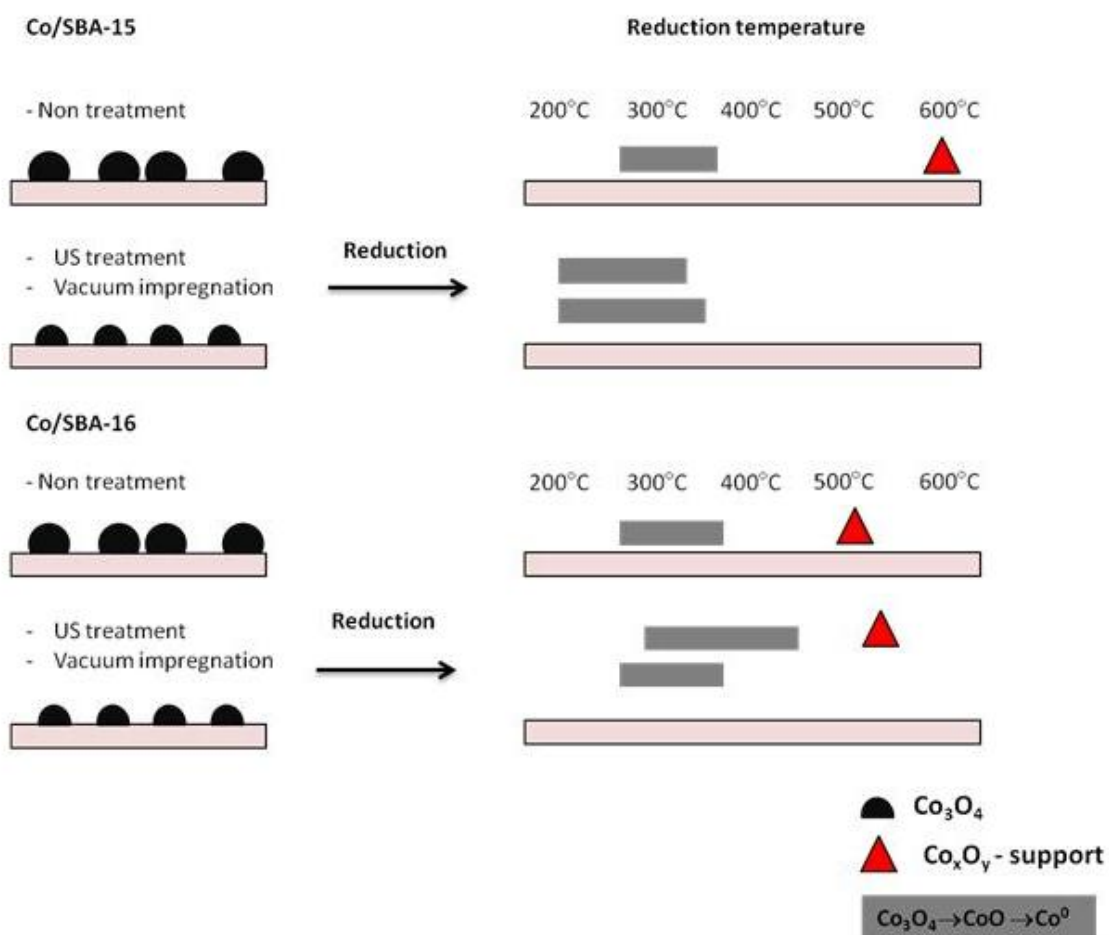


Figure 4.7 XRD patterns of Co/SBA-16-N catalyst

(a) before reduction (b) after reduction



Scheme 1 Conceptual model for reduction of Co/SBA-15 and Co/SBA16

4.1.6 Reaction study

The simple CO₂ hydrogenation under methanation was used to investigate the catalytic properties. The CO₂ conversion and selectivity are presented in **Table 4.3**. Products were collected at initial state (10 min after reaction starting) and steady state (6 h after starting), which mostly consist of CH₄ and CO. From the results, catalysts under the vacuum treatment exhibited the highest activity for both Co/SBA-15 and Co/SBA-16 catalysts, while for the US treatment only Co/SBA-15 showed higher activity. The catalytic properties are obviously related to the TPR results as mentioned above. The strong metal-support interaction can result in poor activity. This may be due to the difficultly reduced catalysts regarding the presence of many cobalt inactive species (Co²⁺). It has been suggested in the previous report [44] that Co²⁺ is an inactive species that performed highly interaction between metal and support, which is CoSiO₄ or cobalt silicate. Therefore, from TPR results, low metal-support interaction catalysts have high catalytic activity due to their high active cobalt species. Based on this study, it revealed that the CO₂ conversion increases in the order of vacuum > US > none treatment.

Table 4.3 CO₂ hydrogenation results for Co/SBA-15 and Co/SBA-16 catalysts

catalyst	Conversion (%)	Rate ($\times 10^2$ g_{CH₄}·g_{cat}⁻¹·h⁻¹)
Co/SBA-15-N	3.9	2.49
Co/SBA-15-U	8.1	5.22
Co/SBA-15-V	9.6	6.59
Co/SBA-16-N	3.0	1.89
Co/SBA-16-U	3.6	2.32
Co/SBA-16-V	14.4	8.99

Reaction condition: 220°C, 1 atm, H₂/CO₂ = 10:1. The conversion and activity based on the amount of methane formation. Conversion and activity were determined after running for 6 h.

4.2 The promoting effects of ceria on Co/SBA-15 catalysts

This part describes the promoting effects of ceria modified Co/SBA-15 catalyst by co-impregnation and sequential impregnation. The catalyst characterization results using various techniques including SEM/EDX, XRD and TPR are given in section 4.2.1-4.2.3 and section 4.2.4 describes the catalytic performance.

4.2.1 Scanning Electron Microscope and Energy-dispersive X-ray spectroscopy (SEM/EDX)

SEM combined with EDX spectroscopy was used to determine the distribution of cobalt and ceria. Table 4.4 summarizes metal distribution and Co_3O_4 crystallite size determined by XRD technique. The results showed that ceria promoted Co/SBA-15-N catalyst exhibited higher metal distribution than unpromoted catalysts due to its small cobalt oxide size. This is because the Co_3O_4 crystallite size is inversely proportional to the metal distribution. As the size of the crystallites decreased, the dispersed metal is increased. However, the preparation method not seems to be the main factor affecting on an increase in the metal distribution for none post-impregnation treatment catalysts. Both of impregnation methods gave high metal distribution. Nevertheless, catalysts prepared by co-impregnation exhibited quite lower distribution than sequentially impregnating catalysts.

As described in Section 4.1, ultrasound and vacuum impregnation increases the metal distribution. Then, post-impregnation treatments were also applied in order

to study the effects of the post-impregnation treatment on the promoted catalysts. It is seen in Table 4.4 that Co/SBA-15-U exhibited the highest cobalt distribution because of the smallest Co_3O_4 crystallites, when compared to Co-Ce/SBA-15-U and Co/Ce-SBA-15-U. When ceria promotion was applied, both impregnation methods showed a decrease in cobalt distribution. This is may be because of the partial physical blockage by the promoter .

For the catalysts using vacuum impregnation as the post-impregnation treatment, the impregnation method seems to be a significant factor. Co-impregnation and sequential impregnation gave two different results. Co-Ce/SBA-15-V exhibited lower cobalt distribution than Co/SBA-15-V, while Co/Ce-SBA-15-V gave higher cobalt distribution than Co/SBA-15-V. This was in accordance with the crystallite size. The crystallite size shows an increase when decreasing the metal distribution. Therefore, for vacuum impregnation catalysts, Co/Ce-SBA-15-V gave the highest metal distribution due to smallest Co_3O_4 crystallites.

Table 4.4 Cobalt oxides distribution and their crystallite size of CeO₂-promoted Co/SBA-15 catalysts

Post-impregnation method	catalysts	wt% Cobalt on support ^a	wt% Ceria on support ^a	Cobalt oxide crystallite size (nm) ^b
Non treatment	Co/SBA-15-N	28.2	0.0	28.8
	Co-Ce/SBA-15-N	31.3	9.1	17.6
	Co/Ce-SBA-15-N	34.4	8.8	14.1
Ultrasound treatment	Co/SBA-15-U	45.9	0.0	13.0
	Co-Ce/SBA-15-U	34.1	11.6	20.2
	Co/Ce-SBA-15-U	32.3	13.1	19.1
Vacuum impregnation	Co/SBA-15-V	38.5	0.0	17.7
	Co-Ce/SBA-15-V	25.1	12.3	22.6
	Co/Ce-SBA-15-V	40.3	14.5	16.0

^a EDX analysis

^b XRD analysis

4.2.2 X-ray diffractation (XRD)

The XRD patterns of the ceria promoted Co/SBA-15 catalysts recorded from 15 to 80 of 2θ (degree) are shown in Figure 4.8. The XRD patterns exhibited strong diffraction peaks at $2\theta = 19, 31.3, 36.9, 44.9, 59.4, 65.3$ due to the presence of Co_3O_4 phase. Moreover, the XRD patterns also indicated the CeO_2 phase at $2\theta = 28.6, 47.5, 56.4$. It can be seen that none of the XRD patterns indicated any peak other than Co_3O_4 and CeO_2 . After the post-impregnation treatments and the ceria addition were applied, the peaks assigning to Co_3O_4 and CeO_2 were observed. This confirmed that Co_3O_4 and CeO_2 were retained after loading the ceria and cobalt with different preparation methods.

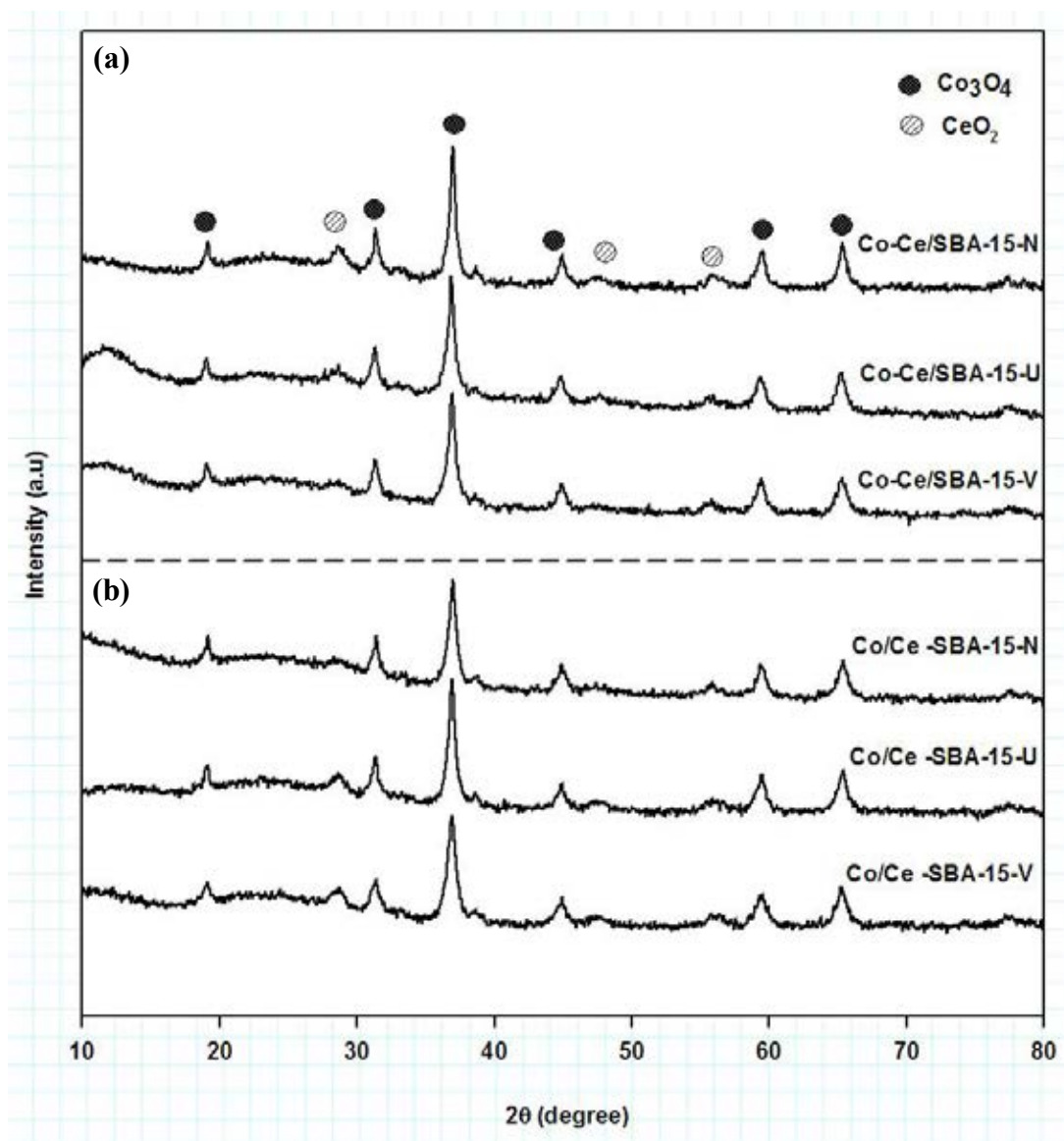


Figure 4.8 XRD patterns of ceria promoted Co/SBA-15 catalysts prepared by
(a) co-impregnation (b) sequential impregnation

4.2.3 Temperature-programmed reduction (TPR)

TPR profiles of ceria promoted and unpromoted Co/SBA-15 catalysts are presented in Figure 4.9. There are two strong peaks observed. The first peak is attributed to the reduction of Co^{3+} to Co^{2+} . The second peak is related to the reduction of Co^{2+} to Co^0 . Hydrogen consumptions at the peak temperatures are measured by the area under the peaks. It is clear that ceria significantly affected the amount of hydrogen used. The area under the curve of ceria promoted catalysts was higher than unpromoted catalysts. Moreover, the metal-support interaction occurring at high temperature ($>500^\circ\text{C}$) was observed only in case of Co/SBA-15-N. TPR profiles of ceria promoted Co/SBA-15-N catalysts did not reveal any the metal-support interaction. It can be concluded that the ceria promotion increased the reducibility of the catalyst and decreased the metal-support interaction. This is because the presence of ceria greatly reduced the Co_3O_4 crystallites. As described in Section 4.1, the metal-support interaction of Co/SBA-15 catalyst is weak interaction. The promoted catalysts showed Co_3O_4 crystallites smaller than the unpromoted catalyst, and hence easier to reduce.

Promoted catalysts, which the ultrasound treatment was applied, showed an increase in reducibility. In fact, both of co-impregnation and sequential impregnation resulted in their high reducibility and hydrogen consumptions in the temperature range $200\text{-}500^\circ\text{C}$ of promoted catalysts were very close. Thus, the different preparation methods did not seem to have an effect on the reduction in this

temperature range. Both methods gave higher reducibility than the unpromoted catalyst and no metal-support interaction was found.

Co/SBA-15-V was also modified by ceria. The TPR results showed that the promoted catalysts resulted in a higher reducibility than unpromoted catalyst. However, it was found that the Co/ Ce-SBA-15-V catalyst showed lower metal-support interaction than Co-Ce/ SBA-15-V. This result indicates that the preparation methods become more significant if vacuum impregnation treatment and ceria is used together. The catalyst prepared by sequential impregnation resulted in decrease of interaction, while co-impregnation resulted in increase of interaction. This might be because Co-Ce/ SBA-15-V exhibited rather large crystallite sizes. Co/SBA-15 is a weak metal-support interaction. The Co-Ce/ SBA-15-V catalyst has a larger size, and then it is harder to reduce.

As described in Section 4.1, the post-impregnation treatments improved a decrease in the metal-support interaction. However, when the post-impregnation treatments were applied on the promoted catalyst, it did not serve the best results in reduced metal-support interaction as seen in the case of Co-Ce/ SBA-15-V. Therefore, an efficient method to synthesize good catalyst would be either promoted by ceria or post-impregnation treatments.

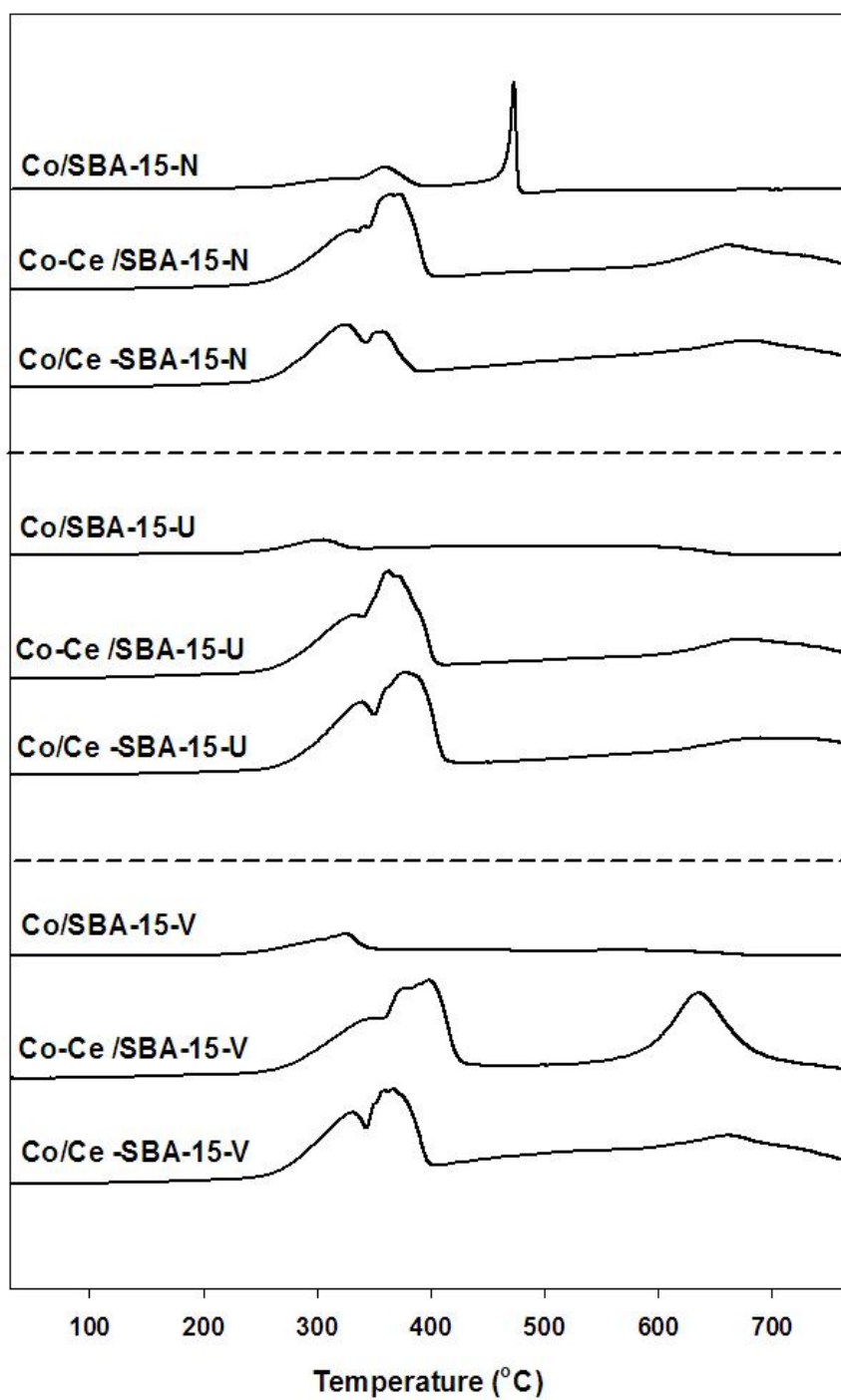


Figure 4.9 TPR patterns of Co/SBA-15 and ceria promoted Co/SBA-15 catalysts with post-impregnation treatment

4.2.4 Reaction study

The catalytic performances of ceria promoted Co/SBA-15 catalysts are summarized in Table 4.5. The results from the activity tests of Co/SBA-15 are also presented to explain the effect of ceria addition and the effect of different preparation methods. All catalysts indicated a very small variation in selectivity. Hence, the conversion calculation is based on mole of methane produced, which is more than 99% of all products. From Table 4.5, it can be seen that all promoted catalysts exhibited an increase in activity. The catalytic activity increased in the order: Co/Ce-SBA-15-N > Co-Ce/SBA-15-N > Co/SBA-15-N. The increased catalytic activity is therefore mostly due to enhancing cobalt distribution and reducing metal-support interaction, as compared to Co/SBA-15-N.

Co/SBA-15-U catalyst was modified by co-impregnation and sequential impregnation to study the catalytic activity for CO₂ hydrogenation reaction. The results reported in Table 4.5 indicated that the catalyst prepared by co-impregnation performed better performance than that catalyst prepared by sequential impregnation. Their catalytic performance is dependent on the enhancement of Co₃O₄ distribution, cobalt crystallite size and the metal-support interaction. Both cases have similar in size and low metal-support interaction. The increased in the activity of the Co-Ce/SBA-15-U is suggested to be due to high cobalt distribution [45].

As described in Section 4.1, the vacuum impregnation decreased the metal-support interaction. When vacuum-impregnation was applied on ceria promoted catalysts, the Co-Ce /SBA-15-V catalyst showed the highest metal-support interaction. This may be correlated to the fact that the Co/Ce-SBA-15-V catalyst

showed higher activity than the Co-Ce /SBA-15-V catalyst. On the other hand, the Co/SBA-15-V catalyst exhibited the lowest activity because the reducibility was very low. It is clear that the effect of ceria addition is more pronounced than the post-impregnation treatments because it can also increase the reducibility and decrease the metal-support interaction.

Table 4.5 The catalytic activity of ceria promoted Co/SBA-15 catalysts

Post-impregnation method	catalyst	Conversion (%)	Activity ($\times 10^2 \frac{\text{g CH}_4}{\text{l} \cdot \text{h}} \cdot \text{g}_{\text{cat}}^{-1}$)
Non treatment	Co/SBA-15-N	3.9	2.49
	Co-Ce/ SBA-15-N	20.5	12.0
	Co/Ce -SBA-15-N	26.7	17.6
Ultrasound treatment	Co/SBA-15-U	8.1	5.22
	Co-Ce/ SBA-15-U	22.1	13.7
	Co/Ce -SBA-15-U	20.1	13.1
Vacuum impregnation	Co/SBA-15-V	9.6	6.59
	Co-Ce/ SBA-15-V	13.6	8.56
	Co/Ce -SBA-15-V	21.0	12.9

Reaction condition: 493K, 1 atm, $\text{H}_2/\text{CO}_2 = 10:1$. The conversion and activity based on the amount of methane formation. Conversion and activity were determined after running for 6 h.

4.3 The promoting effects of ceria on Co/SBA-16 catalysts

4.3.1 Scanning Electron Microscope and Energy-dispersive X-ray spectroscopy (SEM/EDX)

SEM/EDX of ceria promoted Co/SBA-16 catalysts with different preparation method is shown in Table 4.6. The crystallite size of Co_3O_4 is also tabulated as seen in Table 4.6. The unpromoted catalysts showed the highest metal distribution. It is worth to noticing that the ceria added does not respect to Co/SBA-16 catalysts. In case of ceria promoted catalysts, the cobalt distribution is decrease due to the partial physical blockage by the promoter. Further decrease in metal distribution results an increase in crystallite size. The cobalt distribution is increased in order of;

(i) Non-treatment catalysts

$\text{Co/SBA-16-N} > \text{Co/ Ce-SBA-16-N} > \text{Co-Ce /SBA-16-N}$

(ii) US treatment catalysts

$\text{Co/SBA-16-U} > \text{Co-Ce /SBA-16-U} > \text{Co/ Ce-SBA-16-U}$

(iii) Vacuum impregnation catalysts

$\text{Co/SBA-16-V} > \text{Co/ Ce-SBA-16-V} > \text{Co-Ce /SBA-16-V}$

Table 4.6 the cobalt distribution and the Co_3O_4 crystallite size of CeO_2 -promoted Co/SBA-16 catalysts

Post-impregnation method	catalysts	wt% Cobalt distribution ^a	wt% Ceria distribution ^a	Cobalt oxide crystallite size (nm) ^b
Non treatment	Co/SBA-16-N	49.2	0.0	14.6
	Co-Ce/SBA-16-N	40.9	11.7	33.1
	Co/Ce-SBA-16-N	45.6	6.59	18.2
Ultrasound treatment	Co/SBA-16-U	75.8	0.0	23.8
	Co-Ce/SBA-16-U	43.3	12.8	26.6
	Co/Ce-SBA-16-U	42.6	7.0	36.7
Vacuum impregnation	Co/SBA-16-V	49.4	0.0	16.7
	Co-Ce/SBA-16-V	39.5	12.1	27.5
	Co/Ce-SBA-16-V	42.6	10.2	22.1

^a EDX analysis

^b XRD analysis

4.3.2 X-ray diffraction (XRD)

Figure 4.10 shows the XRD patterns of ceria promoted Co/SBA-16 catalysts. The diffraction pattern contains peaks similar to ceria promoted Co/SBA-15 catalysts confirming Co_3O_4 and CeO_2 phases. After the post-impregnation treatments and the ceria addition were applied, the peaks corresponding to the Co_3O_4 and CeO_2 phases are detected. Therefore, the post-impregnation treatment does not form the other phases.

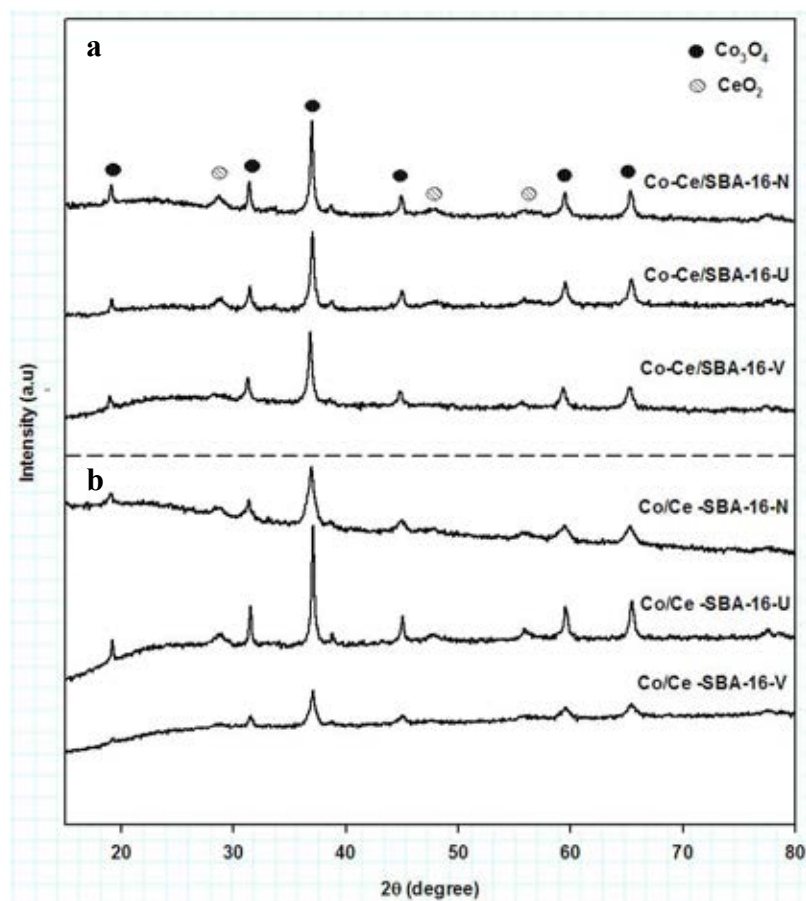


Figure 4.10 XRD patterns of ceria promoted Co/SBA-16 catalysts prepared by (a) co-impregnation (b) sequential impregnation

4.3.3 Temperature-programmed reduction (TPR)

TPR experiments were performed to study the reduction behavior. TPR profiles of ceria promoted catalysts are shown in Fig. 4.11. There are two strong peaks in the TPR profiles. The first peak is attributed to the reduction of Co_3O_4 to CoO . The second peak is for the stepwise reduction of CoO to metallic cobalt. The last peak is due to the reduction of metal-support compounds. After post-impregnation treatment step, the H_2 consumption peaks corresponding to the reduction of Co_3O_4 could be still observed in the TPR profiles, but changed in positions.

In the TPR profile of non-treatment catalysts, Co/SBA-16-N exhibited low reducibility and strong metal-support interaction. At the same time, ceria promoted catalysts exhibited high reducibility and very weak of metal-support interaction indicating decrease of metal-support interaction and increase of reducibility.

In the case of US treatment catalysts, Co/SBA-16-U also served high metal-support interaction. After catalysts were promoted by ceria, TPR profiles displayed high H_2 consumption. However, the onset temperatures of Co/Ce-SBA-16-U were shifted to higher values and have high metal-support interaction, suggesting that the ceria is hindered. But for Co-Ce/SBA-16-U catalyst, there is no metal-support interaction observed. Thus, the preparation method mainly affected on the reduction behavior and metal-support interaction. Co-impregnation results in more reducibility and no metal-support interaction.

TPR result of vacuum impregnation catalysts was also studied. Although the treated catalyst did not modify by ceria, it exhibited low metal-support interaction. When ceria was added, the metal-support interaction is disappeared completely. It is interesting that sequential impregnation method performed finely dispersed cobalt species. This is confirmed by a broad peak around 250-400 °C. However, the modifications are not significant enough. The treated catalyst served a good reduction behavior.

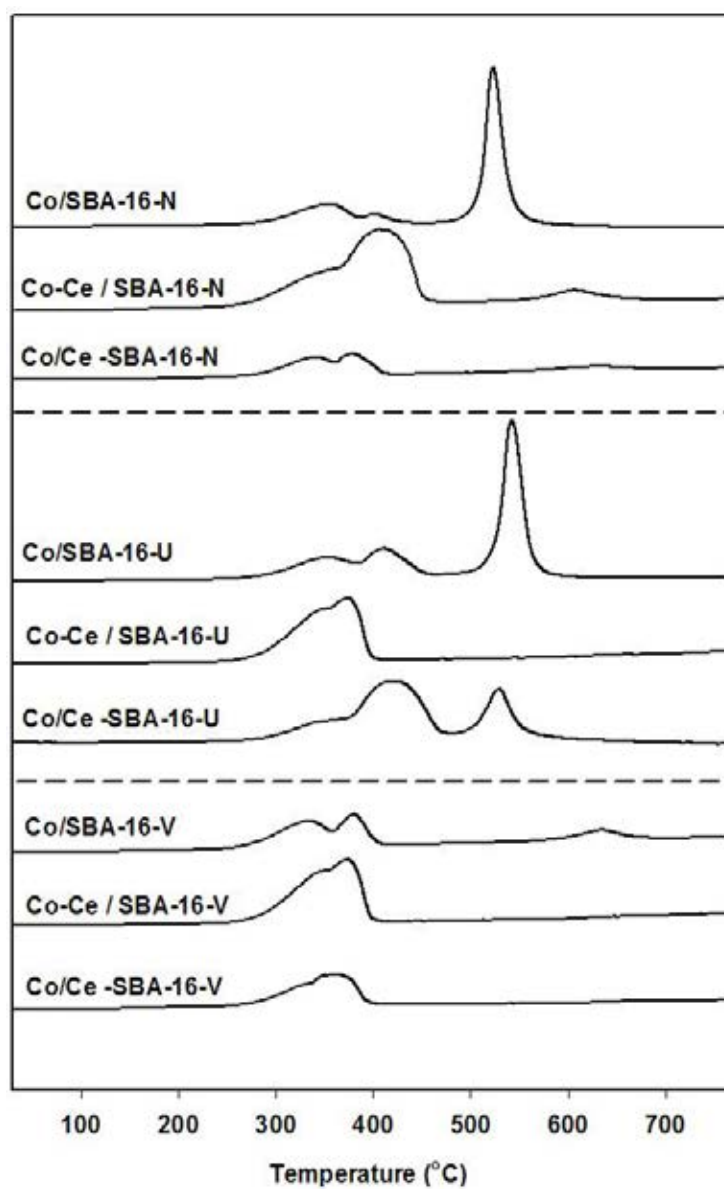


Figure 4.11 TPR patterns of Co/SBA-16 and ceria promoted Co/SBA-16 catalysts with post-impregnation treatment

4.3.4 Reaction study

Catalytic performances of the prepared catalysts are shown in Table 4.7. No remarkable differences in product composition with catalysts used were observed. The major product obtained was methane. Among non-treatment catalysts, the ceria promoted Co/SBA-16-N catalysts exhibited the highest conversion after operation of 6 h. This is because the Co/SBA-16-N catalyst shows high metal-support interaction resulting in the lowest conversion.

The ceria promoted Co/SBA-16-U catalysts clearly exhibited higher activity than Co/SBA-16-U, despite the fact that a weaker metal-support interaction was occurred. One possible is that the larger cobalt crystallites give it easier to reduce. The Co-Ce/ SBA-16-N catalyst, which is produced by the co-impregnation procedure, showed the best catalytic behavior because no metal-support interaction was found.

As in the case of vacuum impregnation, the ceria added did not influence the activity. The catalytic activity of Co/SBA-16-V catalyst is higher than that of the promoted catalysts, which was opposite in the case of non-treatment catalysts and US treatment catalysts. The result is in agreement with TPR result. Low metal-support interaction explains high activity. Although the promoted catalysts have more reducibility than Co/SBA-16-V catalyst, high catalytic performance does not found. It can be inferred that increasing reducibility is not a main key to improve the catalytic performance, but rather is low metal-support interaction.

Table 4.7 The catalytic activity of ceria promoted Co/SBA-15 catalysts

Post-impregnation method	catalyst	Conversion (%)	Activity ($\times 10^2 \text{ g}_{\text{CH}_2} \cdot \text{g}_{\text{cat}}^{-1} \cdot \text{h}^{-1}$)
Non treatment	Co/SBA-16-N	3.0	1.89
	Co-Ce/ SBA-16-N	6.4	3.93
	Co/Ce -SBA-16-N	6.4	3.99
Ultrasound treatment	Co/SBA-16-U	3.6	2.32
	Co-Ce/ SBA-16-U	4.1	2.57
	Co/Ce -SBA-16-U	3.8	2.44
Vacuum impregnation	Co/SBA-16-V	14.4	8.99
	Co-Ce/ SBA-16-V	9.8	6.10
	Co/Ce -SBA-16-V	13.2	7.88

Reaction condition: 493K, 1 atm, $\text{H}_2/\text{CO}_2 = 10:1$. The conversion and activity based on the amount of methane formation. Conversion and activity were determined after running for 6 h.

Discussion

Table 4.8 The comparison of the catalytic performance

Catalyst	Post-impregnation			Ceria promotion combined with post-impregnation		
	N	U	V	No promote	Co-impregnation	Sequential impregnation
Co/SBA-15	○	✓	✓	N ○	✓	✓
				U ○	✓	✓
				V ○	✓	✓
Co/SBA-16	○	✓	✓	N ○	✓	✓
				U ○	✗	✗
				V ○	✗	✗

Notation: ○, standard; ✓, the activity increased; ✗, the activity decreased

The results showed that the addition of either ceria or post treatment step improved the catalytic performance for CO₂ hydrogenation, but only one is preferred. The most active catalyst is believed to be Co/Ce –SBA-15-N due to lack of interaction. This catalyst shows high activity and low metal-support interaction, which directly influences the catalytic activity. Alternatively, high catalytic activity can be induced by the post-impregnation treatment. Without the addition of ceria, the Co/SBA-16-V catalyst is an interesting catalyst. The presence of low metal-support interaction significantly improved its catalytic performance.

CHAPTER V

CONCLUSIONS AND RECOMMENDATION

This chapter presents the conclusions and recommendations for future outlook.

5.1 Conclusions

The general conclusions that can be concluded from the present investigations are the following;

The post-impregnation treatments such as vacuum and ultrasound were employed for the Co /SBA-15 and Co/SBA-16 catalysts. It is revealed that both treatments enhance the cobalt dispersion for the Co/SBA-15 catalyst. However, only the vacuum treatment was suitable for improving the cobalt dispersion for Co/SBA-16. It was suggested that the vacuum and ultrasound treatments probably had two effects; (i) decrease the crystallite size of cobalt oxide species and (ii) decrease the metal-support interaction resulting in more reduced cobalt atoms. As the results, the catalytic activity for CO₂ hydrogenation of catalysts with post-impregnation treatment was increased

Ceria promoted Co/SBA-15 catalysts were synthesized by co-impregnation and sequential impregnation. Their catalytic performances for methanation were investigated. The promoted catalysts showed the higher activity for methanation compared with the relative non-promoted catalyst. It is revealed that the Co/Ce -SBA-

15-N catalyst gave the highest catalytic activity due to small crystallites, high cobalt oxides distribution and low metal-support interaction.

Ceria promoted Co/SBA-16 catalysts have been also investigated their characteristics and catalytic performance. The catalytic activity of the ceria promoted Co/SBA-16 catalysts depended on their metal-support interaction. The most catalytic active catalyst always has low metal-support interaction. The Co/SBA-16-V catalyst is the most active catalyst for methanation. This is because of its small crystallites and low metal-support interaction. Therefore, it can be concluded that a modified two-step treatment (the post-impregnation treatment and ceria promotion) did not serve the best catalytic performance and wasting time to prepare. In case of the Co/SBA-16 catalyst, vacuum impregnation treatment is more pronounced than the effect of ceria addition.

5.2 Recommendations

Further study will be needed to fully understand the effects of time using in US treatment and vacuum impregnation. However, the support properties such as the acidity and structure should be also study.

REFERENCES

- [1] Janlamool J., and others. Ti-Si composite oxide-supported cobalt catalysts for CO₂ hydrogenation. J. Nat. Gas Chem. 20 (2011): 558–564.
- [2] Pirola C., and others. Ultrasound and microwave assisted synthesis of high loading Fe-supported Fischer–Tropsch catalysts. Ultrason Sonochem 17 (2010): 610–616.
- [3] Zhou X., and others. Effect of vacuum impregnation on the performance of Co/SiO₂ Fischer-Tropsch catalyst. J. Nat. Gas Chem 20 (2011): 350–355.
- [4] Khobragade M., and others. Effect of K and CeO₂ promoters on the activity of Co/SiO₂ catalyst for liquid fuel production from syngas. Appl. Energ. 94 (2012): 385-394.
- [5] Zhao D., and others. Triblock Copolymer Syntheses of Mesoporous Silica with Periodic 50 to 300 Angstrom Pores. Science 279 (1998): 548-552.
- [6] Demuth P., and others. Mesoscale porous silica as drug delivery vehicles: Synthesis, characterization, and pH-sensitive release profiles. Microporous Mesoporous Mater 141 (2011): 128–134.
- [7] Asaeda M., and others. Stability and performance of porous silica–zirconia composite membranes for pervaporation of aqueous organic solutions. J. Membr. Sci. 209 (2002): 163–175.
- [8] Guzmán A., and others. Composite Membranes Based on SBA – 15 and SBA – 16 Evaluated at High Temperature and Low Relative Humidity Fuel Cell Conditions. Int. J. Electrochem. Sci. 6 (2011): 4787 - 4797.
- [9] Taguchi A., and others. Ordered mesoporous materials in catalysis. Microporous Mesoporous Mater 77 (2005): 1-45.
- [10] Oscar A., and others. Synthesis and characterization of SBA-3, SBA-15, and SBA-1 nanostructured catalytic materials. J. Colloid Interface Sci. 315 (2007): 184–190.

- [11] Murakami Y., and others. Microporous Silica Particles Prepared by the Salt-Catalytic Sol-Gel Process with Extremely Low Content of Water. J. Sol-Gel Sci. Technol. 29 (2003): 19-24
- [12] Michorczyk P., and others. Preparation and characterization of SBA-1-supported chromium oxide catalysts for CO₂ assisted dehydrogenation of propane. Microporous Mesoporous Mater. 161 (2012): 56-66
- [13] Huo Q., and others. Surfactant Control of Phases in the Synthesis of Mesoporous Silica-Based Materials. Chem. Mater. 8 (1996): 1147-1160.
- [14] Mohamed A., and others. Influence of synthesis temperature on morphology of SBA-16 mesoporous materials with a three-dimensional pore system. Microporous Mesoporous Mater. 129 (2010): 106–111.
- [15] Davidson A. Modifying the walls of mesoporous silicas prepared by supramolecular-templating. Curr. Opin. Colloid Interface Sci. 7 (2002): 92-106.
- [16] Lu Q., and others. Structure and Photoluminescent Properties of ZnO Encapsulated in Mesoporous Silica SBA-15 Fabricated by Two-Solvent Strategy. Nanoscale Res Lett. 4 (2009): 646-654
- [17] Zhao D., and others. Nonionic Triblock and Star Diblock Copolymer and Oligomeric Surfactant Syntheses of Highly Ordered, Hydrothermally Stable, Mesoporous Silica Structures. J. Am. Chem. Soc. 120 (1998): 6024-6036.
- [18] Soler-Illia G.J.D.A.A., and others. Block copolymer-templated mesoporous oxides. Curr. Opin. Colloid Interface Sci. 8 (2003): 109–126.
- [19] Johansson E. Design of mesoporous silica templates for nanoparticle growth. Master's Thesis, Department of Physics, Goteborg university, 2008.
- [20] Wang Y., and others. Synthesis of SBA-15 with different pore sizes and the utilization as supports of high loading of cobalt catalysts. Catal. Today 68 (2001): 3-9.

- [21] Ding Y., and others. Key role of sodium silicate modulus in synthesis of mesoporous silica SBA-15 rods with controllable lengths and diameters. Mater. Lett. 75 (2012): 45-47.
- [22] Lu B., and others. A novel approach for synthesizing ordered mesoporous silica SBA-15. Mater. Res. Bull. 47 (2012): 1301-1305.
- [23] Sun H., and others. Mesostructured SBA-16 with excellent hydrothermal, thermal and mechanical stabilities: Modified synthesis and its catalytic application. J. Colloid Interface Sci. 333 (2009): 317–323.
- [24] Meynen V., and others. Verified syntheses of mesoporous materials. Microporous Mesoporous Mater. 125 (2009): 170–223.
- [25] Sierra L., and others. Formation mechanism and morphology of mesoporous SBA-16 type silica particles prepared with the triblock copolymer surfactant PEO₁₄₀PPO₃₉PEO₁₄₀. Microporous Mesoporous Mater. 124 (2009): 100-109.
- [26] Zhou X., and others. Effect of vacuum impregnation on the performance of Co/SiO₂ Fischer-Tropsch catalyst. Nat. Gas Chem. 20 (2011): 350–355.
- [27] Khodakov AY., and others. Advances in the Development of Novel Cobalt Fischer-Tropsch Catalysts for Synthesis of Long-Chain Hydrocarbons and Clean Fuels. Chem. Rev. 107 (2007): 1692-1744.
- [28] Hu J. Application of Fischer–Tropsch Synthesis in Biomass to Liquid Conversion. Catalysts 2 (2012): 303-326.
- [29] Cai Q., and others. Catalytic properties of the Ru promoted Co/SBA-15 catalysts for Fischer–Tropsch synthesis. Catal. Commun. 9 (2008): 2003–2006.
- [30] Girardon J., and others. Effect of cobalt precursor and pretreatment conditions on the structure and catalytic performance of cobalt silica-supported Fischer–Tropsch catalysts. J. Catal. 230 (2005): 339–352.

- [31] Cai Q., and others. Catalytic properties of the Ru promoted Co/SBA-15 catalysts for Fischer–Tropsch synthesis. Catal. Commun. 9 (2008): 2003–2006.
- [32] Dorner RW., and others. C2-C5+ olefin production from CO₂ hydrogenation using ceria modified Fe/Mn/K catalysts. Catalyst 15 (2011): 88-92.
- [33] Sinfelt J.H. Highly Dispersed Catalytic Materials. Annu. Rev. Mater. Sci. 2 (1972): 641-662
- [34] Guerrero-Ruiz A., and others. Hydrogenation of CO₂ on carbon-supported nickel and cobalt. React. Kinet. Catal. Lett. 29 (1985): 93-99.
- [35] Khodakov A. Y., and others. Fischer-Tropsch synthesis: Relations between structure of cobalt catalysts and their catalytic performance. Catal. Today 144 (2009): 251–257.
- [36] Zhao Y., and others. The kinetic study of light alkene syntheses by CO₂ hydrogenation over Fe-Ni catalysts. Frontiers of Chemical Engineering in China 4 (2010): 153–162.
- [37] Zhang Y., and others. CO and CO₂ hydrogenation study on supported cobalt Fischer–Tropsch synthesis catalysts. Catal. Today 71 (2002): 411–418.
- [38] Cruz A. E. B., and others. Pt and Ni supported catalysts on SBA-15 and SBA-16 for the synthesis of biodiesel. Catal. Today 166 (2011): 111-115.
- [39] Shia L., and others. Studies on surface impregnation combustion method to prepare supported Co/SiO₂ catalysts and its application for Fischer–Tropsch synthesis. Appl. Catal., A 435-436 (2012): 217-224.
- [40] Liu C., and others. Fischer–Tropsch synthesis over cobalt catalysts supported on nanostructured alumina with various morphologies. J. Mol. Catal. A: Chem. 363-364 (2012): 335-342.
- [41] Jongsomjit B., and others. Co-Support compound formation in titania-supported cobalt catalyst. Catal. Lett. 94 (2004): 209-215.

- [42] Panpranot J., and others. Differences in characteristics and catalytic properties of Co catalysts supported on micro- and nano-sized zirconia. Catal. Commun. 7 (2006): 192-197.
- [43] Raróg-Pilecka W., and others. Ammonia synthesis over barium-promoted cobalt catalysts supported on graphitised carbon. J. Catal. 249 (2007): 24-33.
- [44] Martínez A., and others. Fischer–Tropsch synthesis of hydrocarbons over mesoporous Co/SBA-15 catalysts: the influence of metal loading, cobalt precursor, and promoters. J. Catal. 220 (2003): 486-499.
- [45] Basha S. J. S., and others. Effect of Order of Impregnation of Mo and Ni on the Hydrodenitrogenation Activity of NiO-MoO₃/AlMCM-41 Catalyst. Ind. Eng. Chem. Res. 48 (2009): 2774–2780.

APPENDICES

APPENDIX A

CALCULATION FOR CATALYST PREPARATION

To prepare a support with 20%wt cobalt on SBA-15 (Co/SBA-15), cobalt (II) nitrate hexahydrate (98% purity) was used as a precursor. The following calculation was used to determine how much the precursor used. The molecular weight of different elements and compounds are listed below.

	Molecular weight
Cobalt	58.93
Ceria	140.12
Co(NO ₃) ₂ •6H ₂ O	291.03
Ce(NO ₃) ₃ •6H ₂ O	434.23

Based on 1 g catalyst used,

The weight of cobalt = 0.2 g

The weight of SBA-15 = 1-0.2 = 0.8 g

The weight of Co(NO₃)₂•6H₂O would be needed

$$= 291.03 \times \frac{98}{100} \times \frac{0.2}{58.93} = 0.968 \text{ g}$$

The calculation would be as follows for the 5%wt ceria promoted Co/SBA-15 catalyst. Note that cerium (III) nitrate hexahydrate (99.9% purity) was used as a precursor.

Based on 1 g catalyst used,

The weight of ceria = 0.05 g

The weight of SBA-15 = 1-0.05 = 0.95 g

The weight of $\text{Ce}(\text{NO}_3)_3 \cdot 6\text{H}_2\text{O}$ would be needed

$$= 434.23 \times \frac{99.9}{100} \times \frac{0.05}{140.12} = 0.155 \text{ g}$$

APPENDIX B

SEM/EDX RESULTS

The SEM/EDX results as concluded in section 4.1, 4.2 and 4.3 are described in more detail in this appendix. The SEM/EDX technique is usually used to identify the elements on the surface in the range of 500nm-2 μ m and their relative proportions. All catalyst samples were tested using SEM/EDX to determine their element distribution. The results revealed the weight percent of each element on the surface based on 100% of the surface. The SEM/EDX results of all samples are shown below.

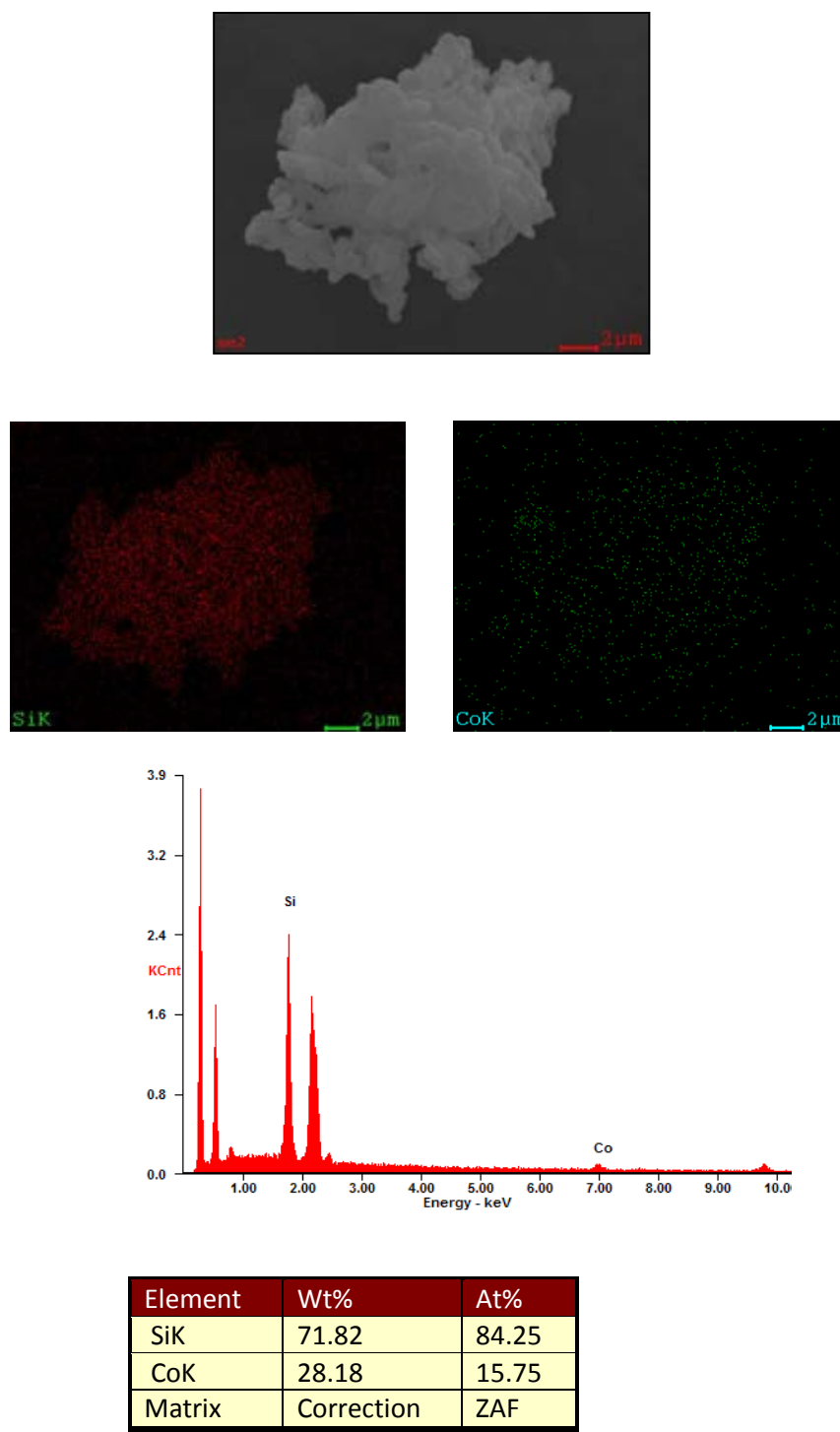


Figure A.1 The SEM/EDX result of Co/SBA-15-N

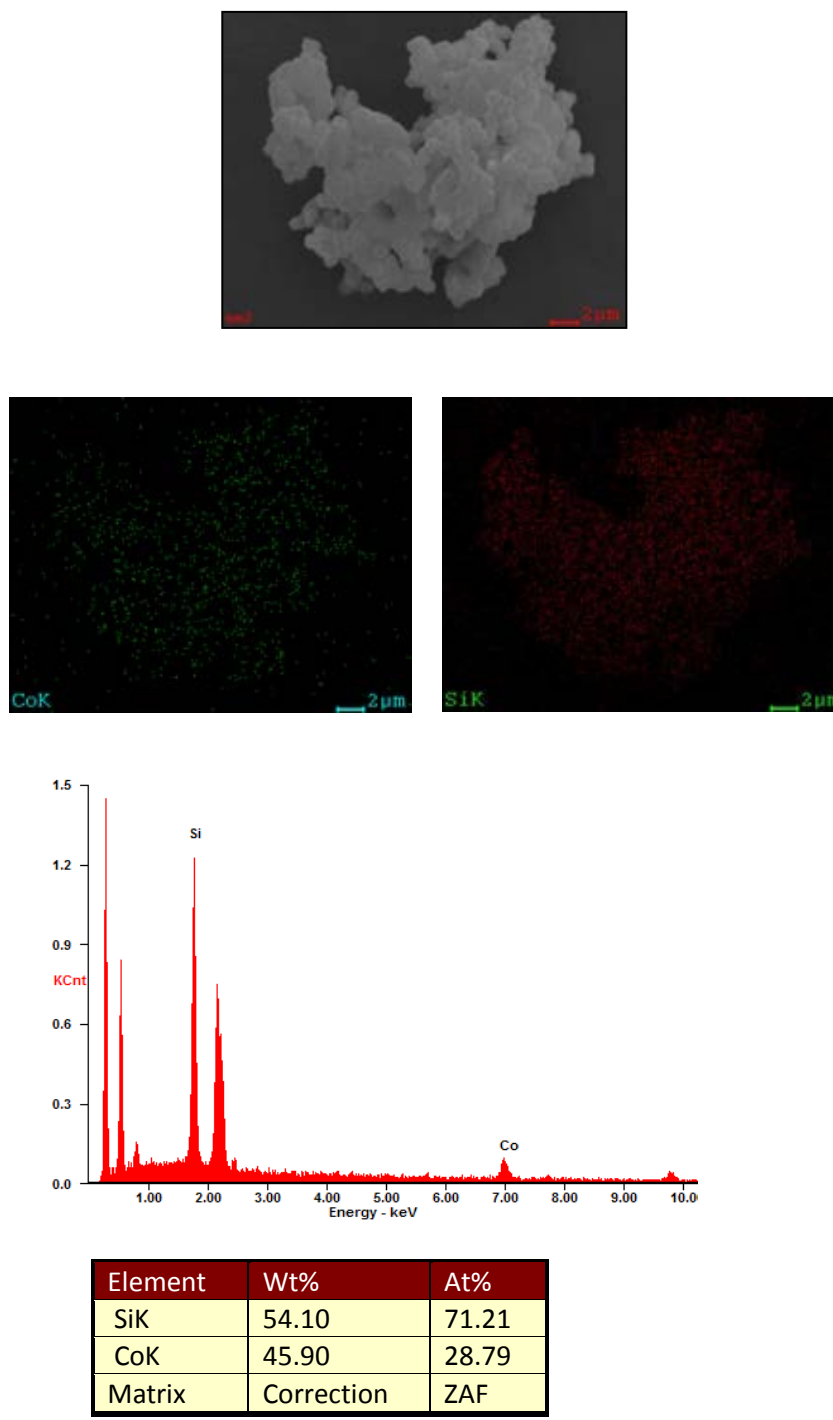


Figure A.2 The SEM/EDX result of Co/SBA-15-U

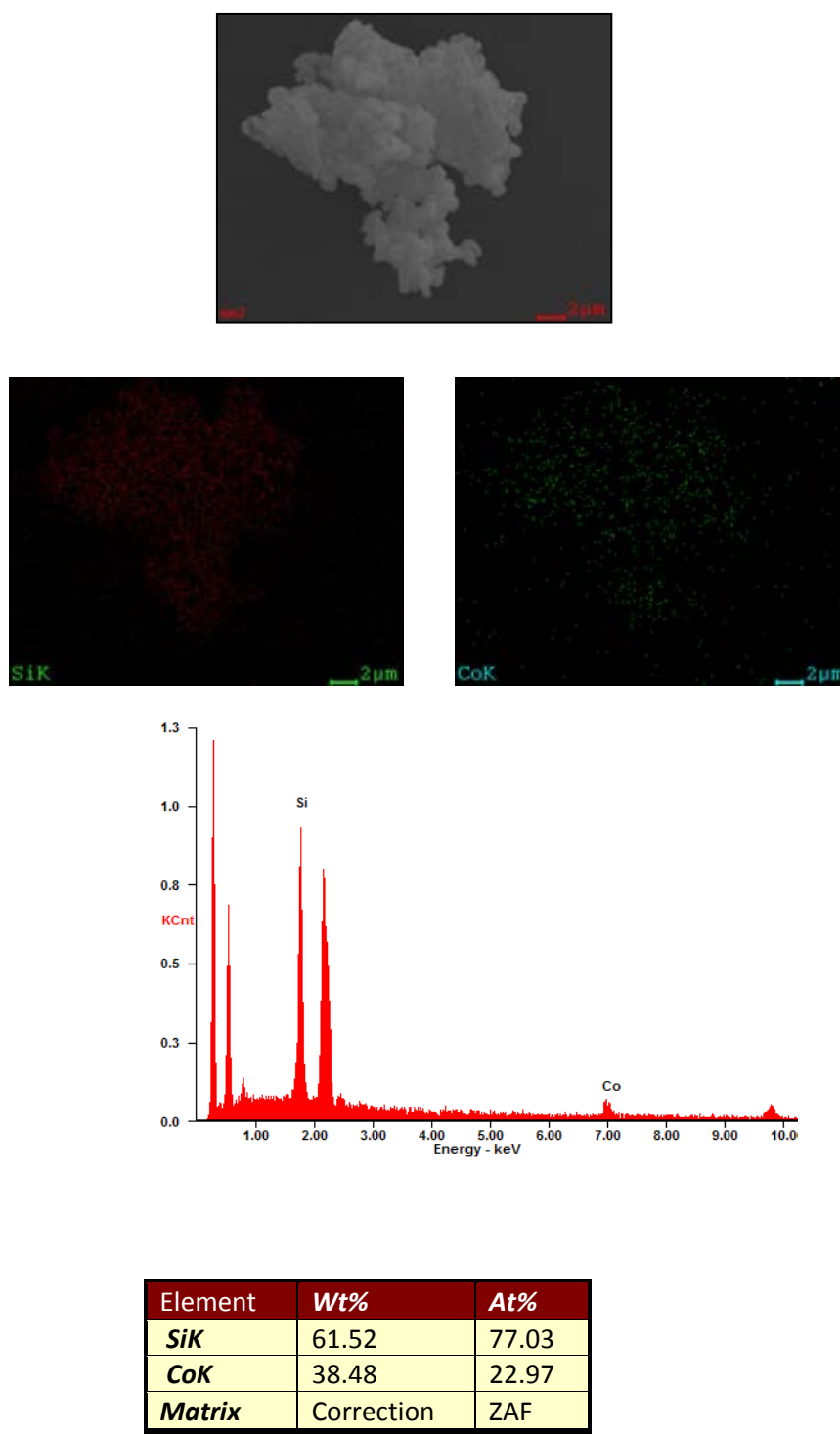


Figure A.3 The SEM/EDX result of Co/SBA-15-V

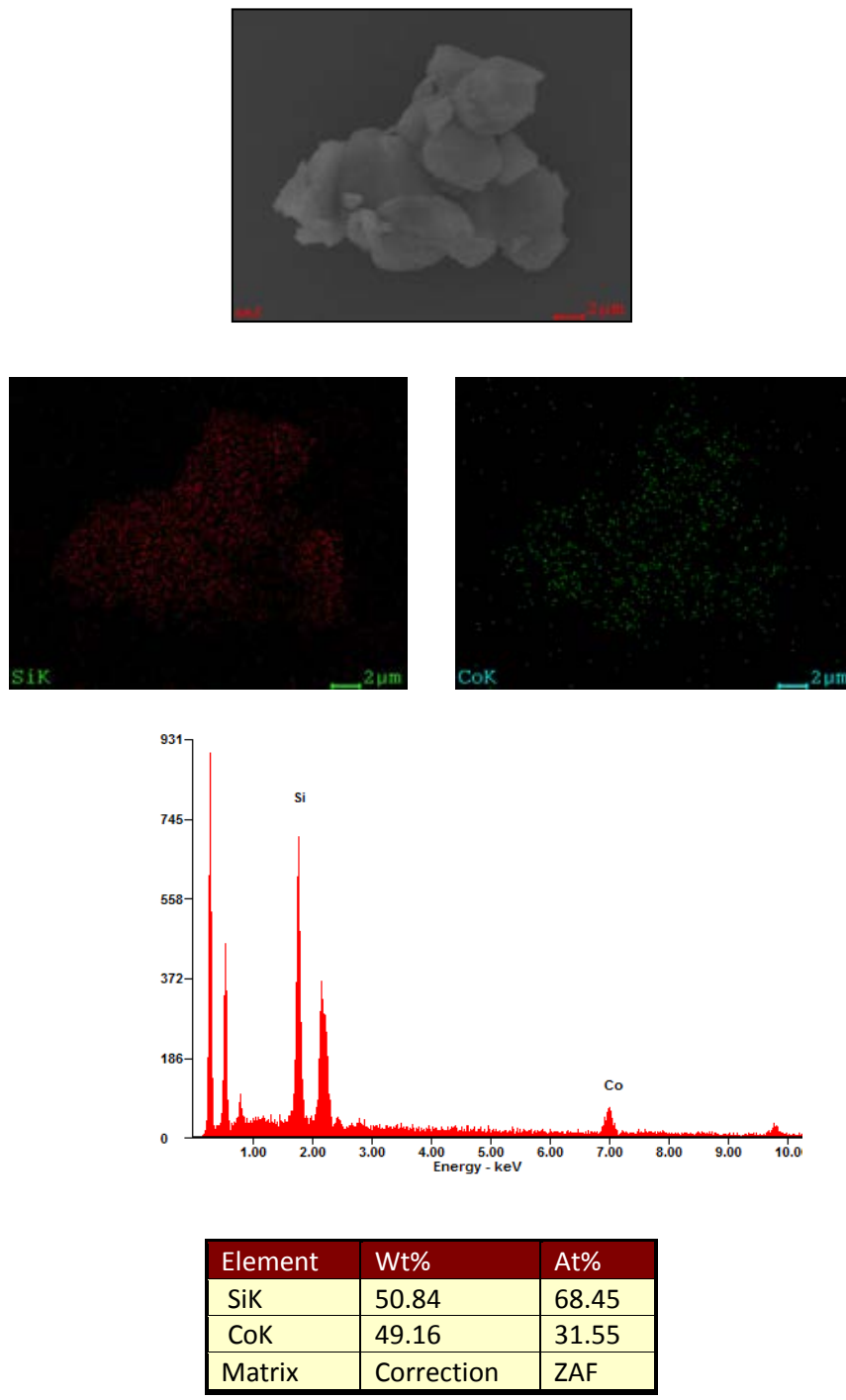


Figure A.4 The SEM/EDX result of Co/SBA-16-N

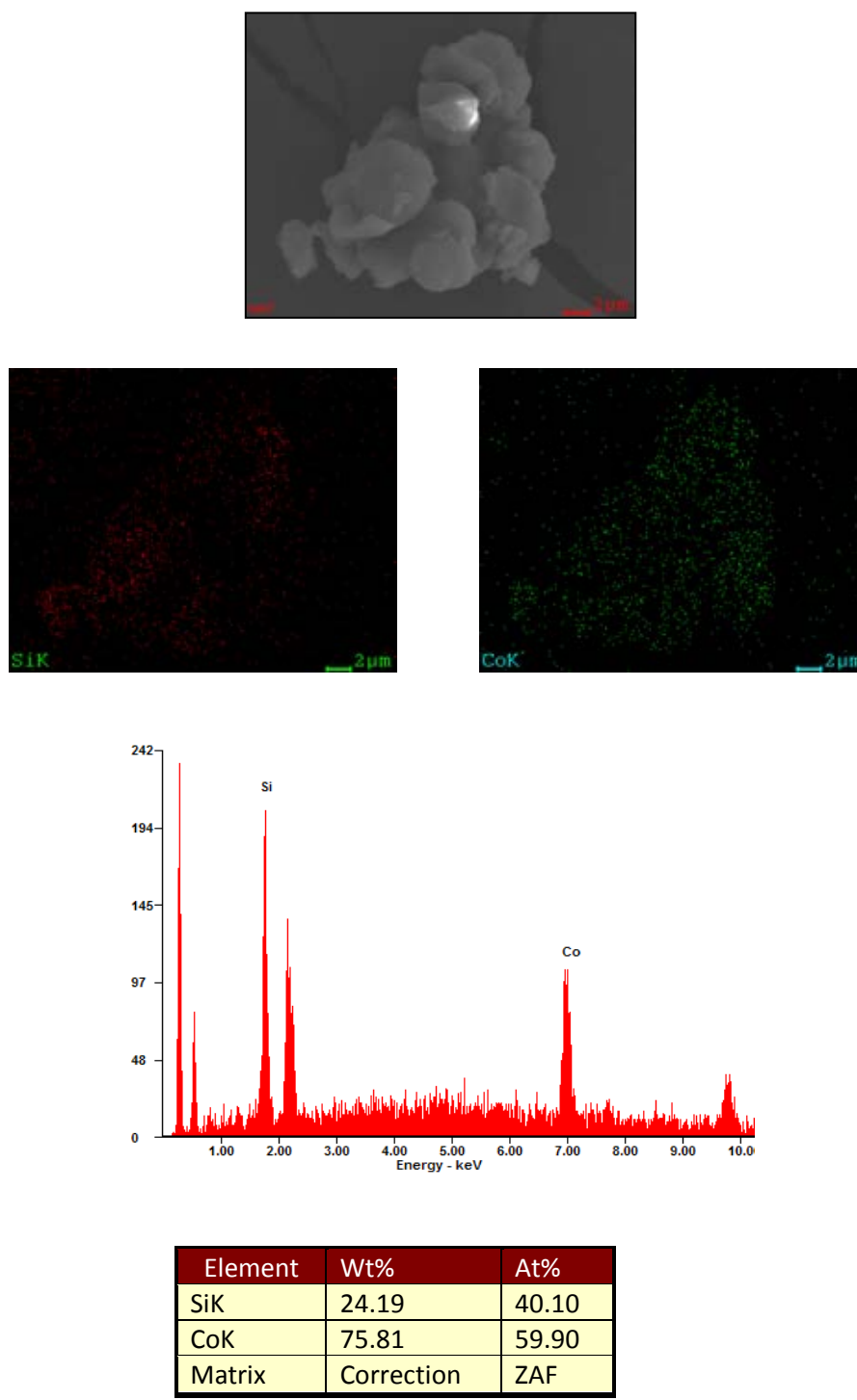


Figure A.5 The SEM/EDX result of Co/SBA-16-U

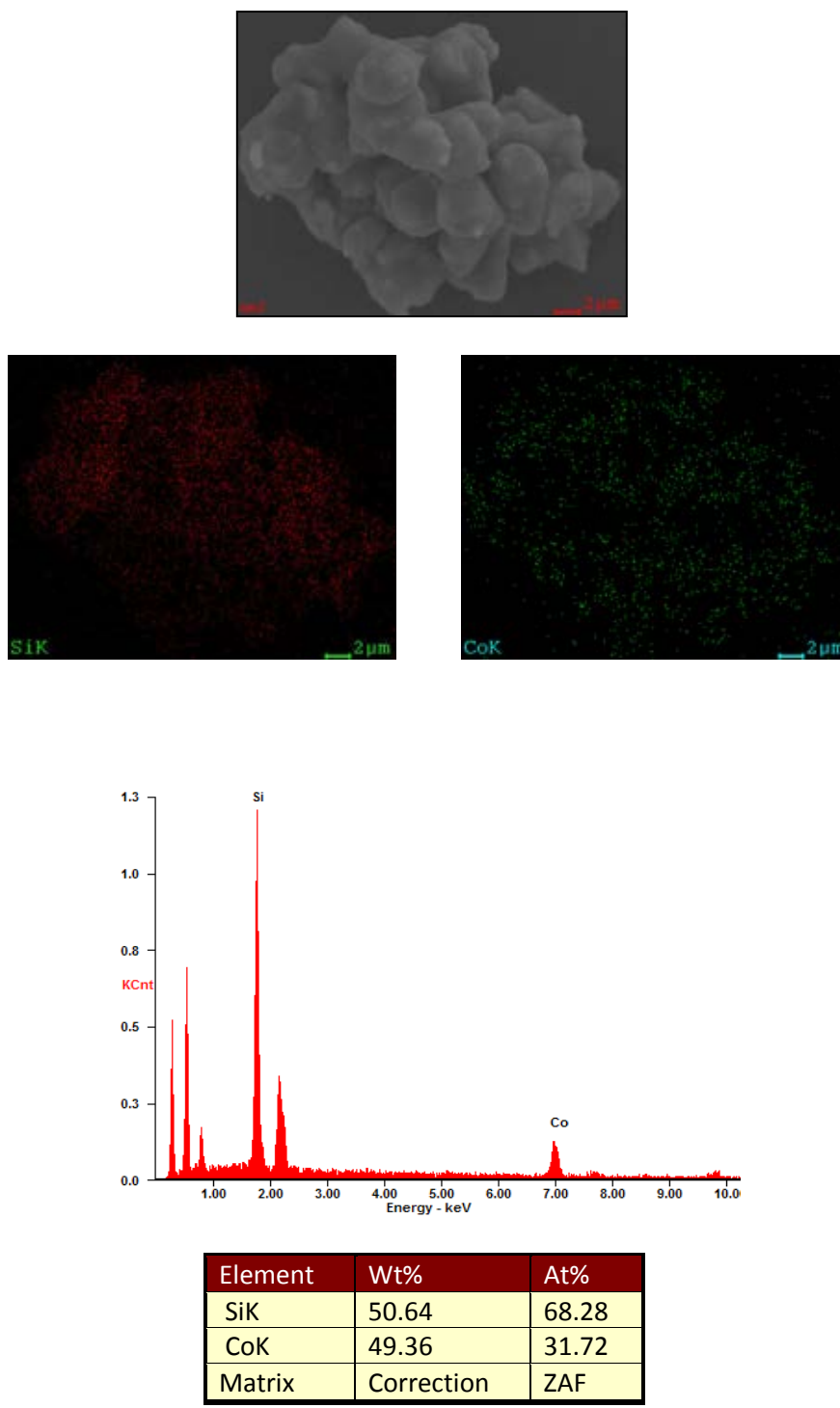
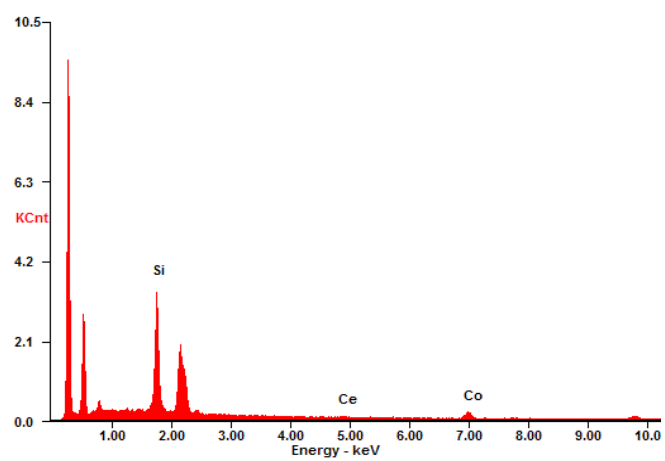
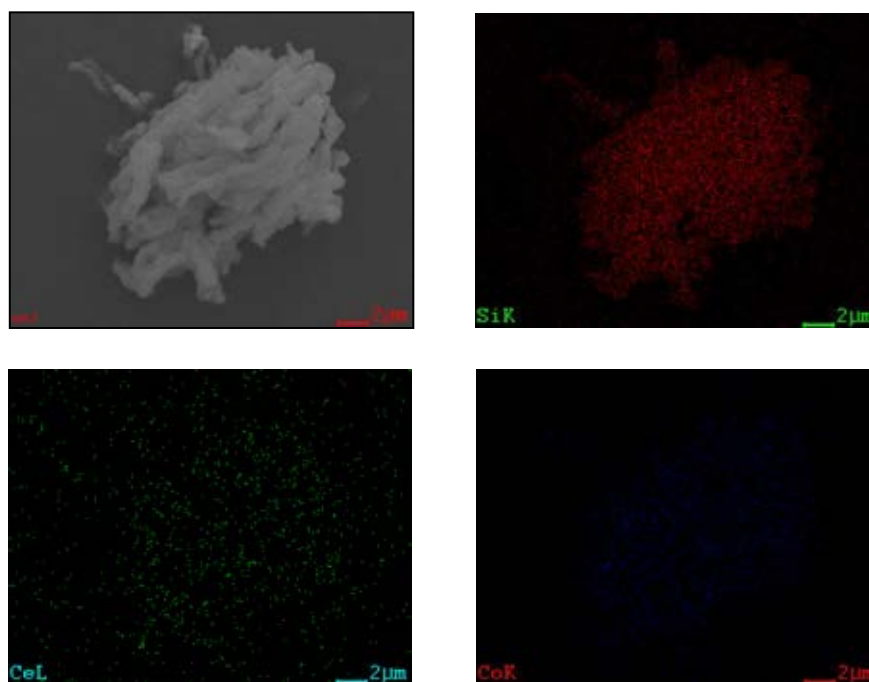
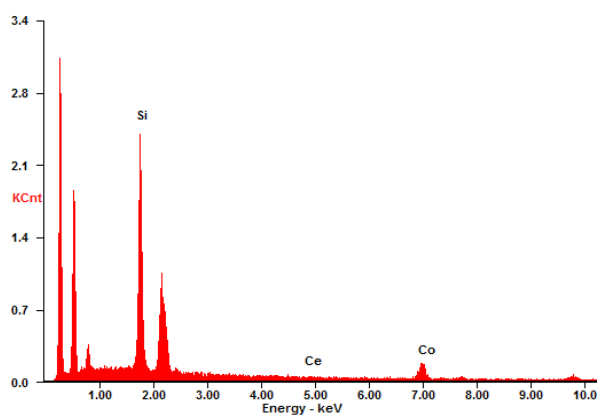
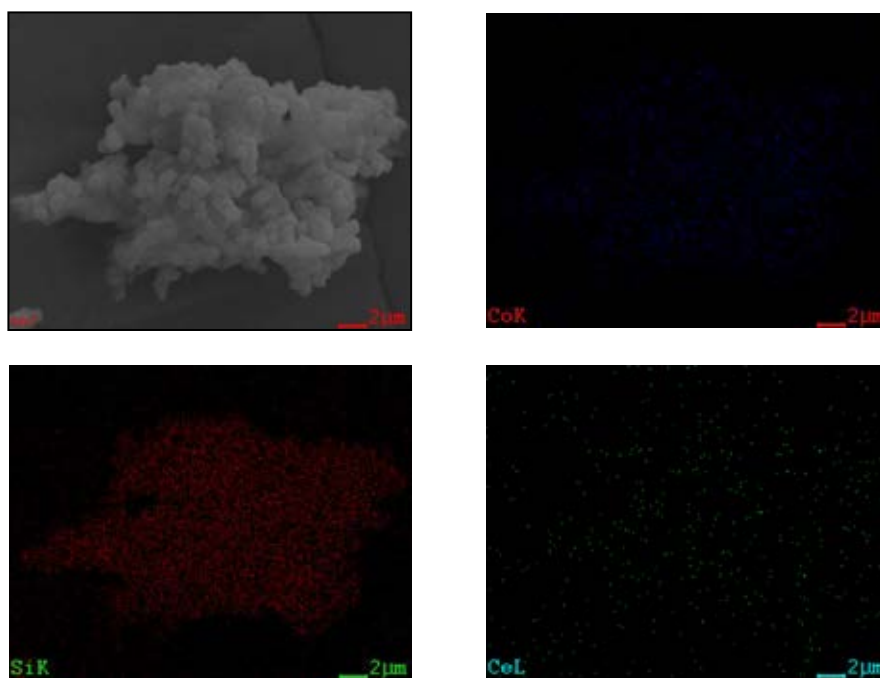


Figure A.6 The SEM/EDX result of Co/SBA-16-V



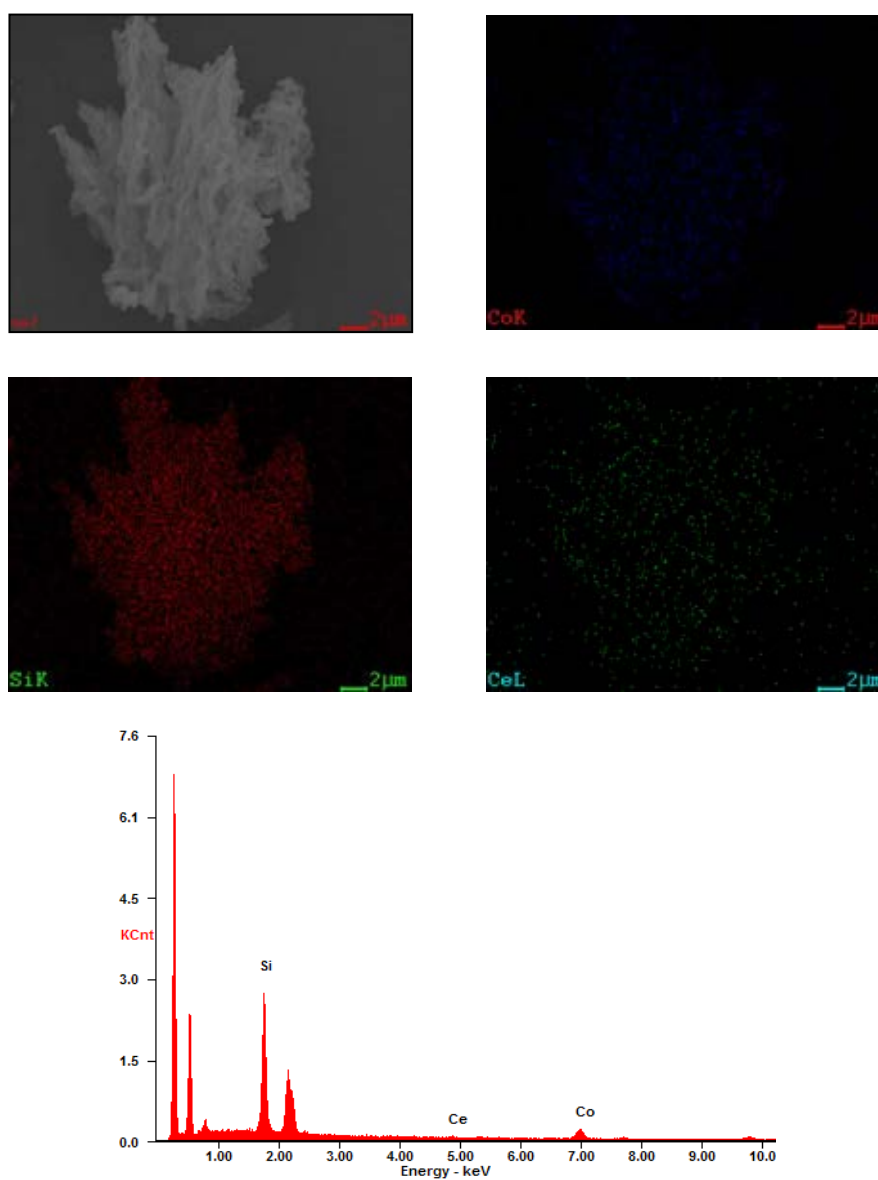
Element	Wt%	At%
SiK	59.54	78.03
CeL	09.11	02.39
CoK	31.34	19.57
Matrix	Correction	ZAF

Figure A.7 The SEM/EDX result of Co-Ce /SBA-15-N



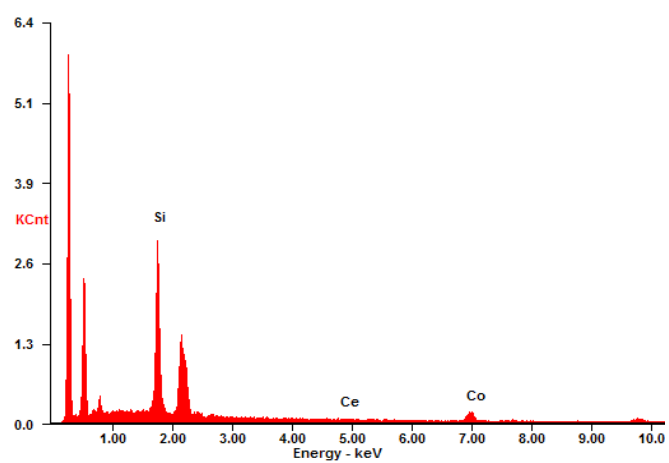
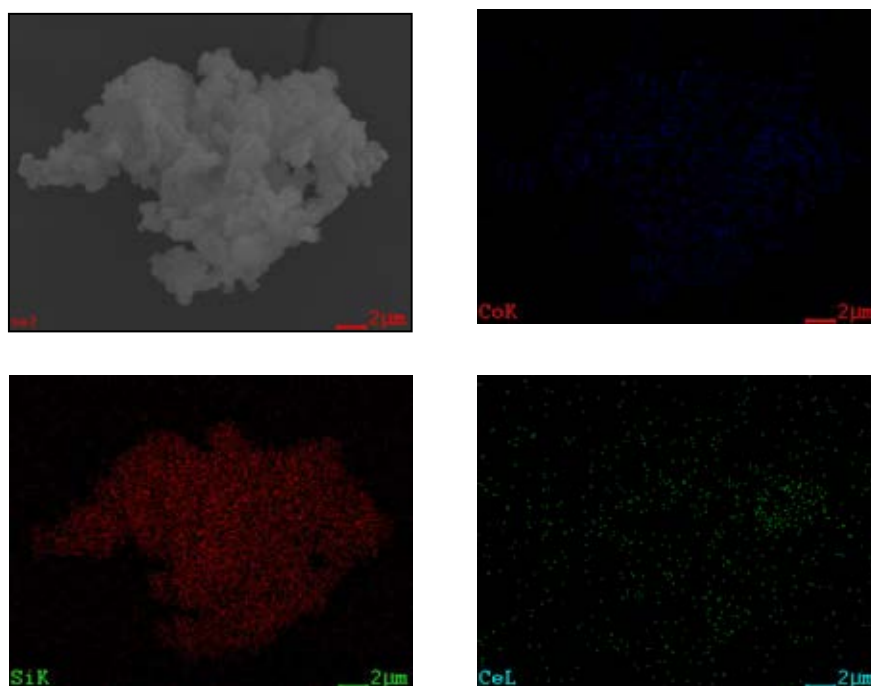
Element	Wt%	At%
<i>SiK</i>	56.80	75.78
<i>CeL</i>	08.83	02.36
<i>CoK</i>	34.37	21.85
<i>Matrix</i>	Correction	ZAF

Figure A.8 The SEM/EDX result of Co/Ce -SBA-15-N



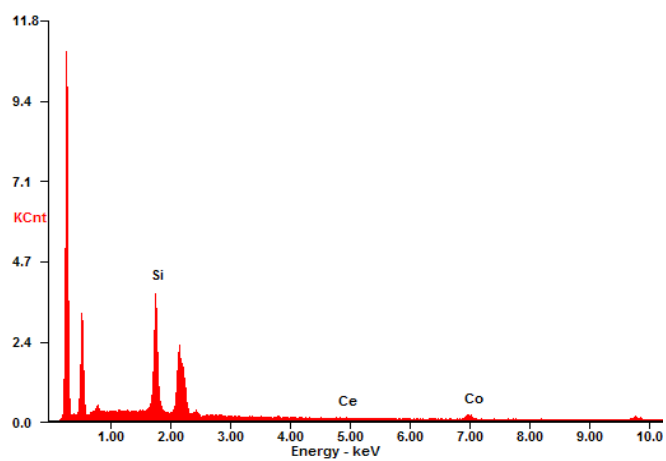
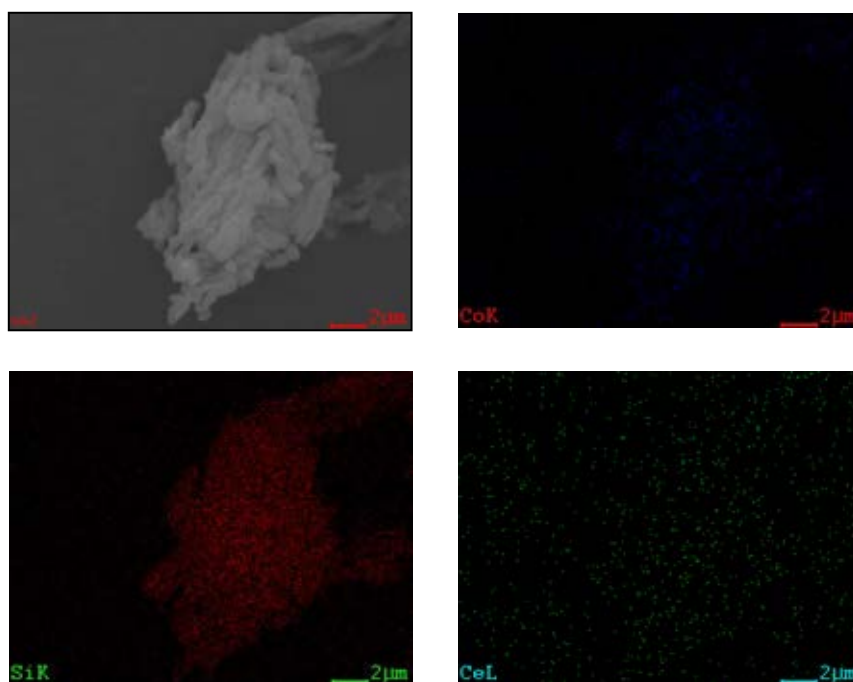
Element	Wt%	At%
SiK	54.59	75.18
CeL	13.11	03.62
CoK	32.30	21.20
Matrix	Correction	ZAF

Figure A.9 The SEM/EDX result of Co-Ce /SBA-15-U



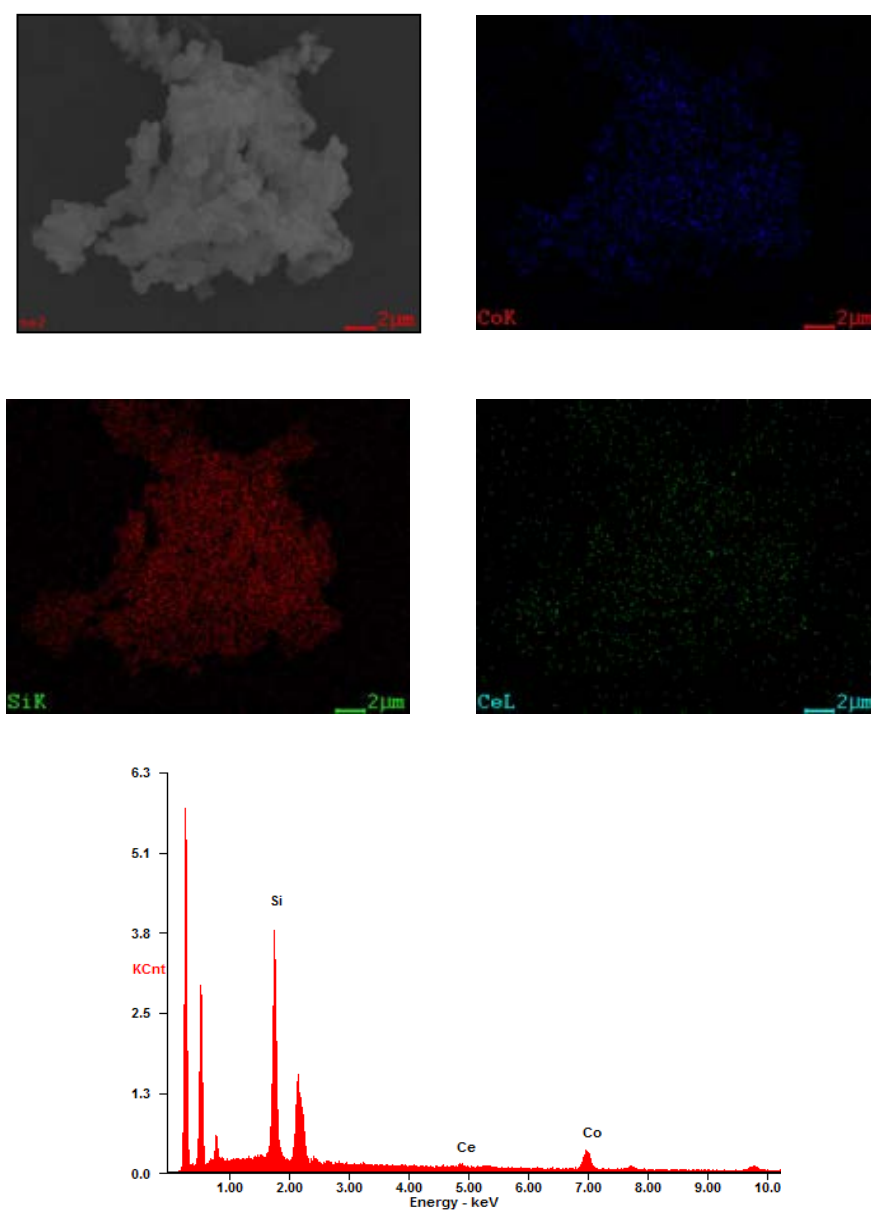
Element	Wt%	At%
SiK	54.29	74.51
CeL	11.64	03.20
CoK	34.07	22.28
Matrix	Correction	ZAF

Figure A.10 The SEM/EDX result of Co/Ce -SBA-15-U



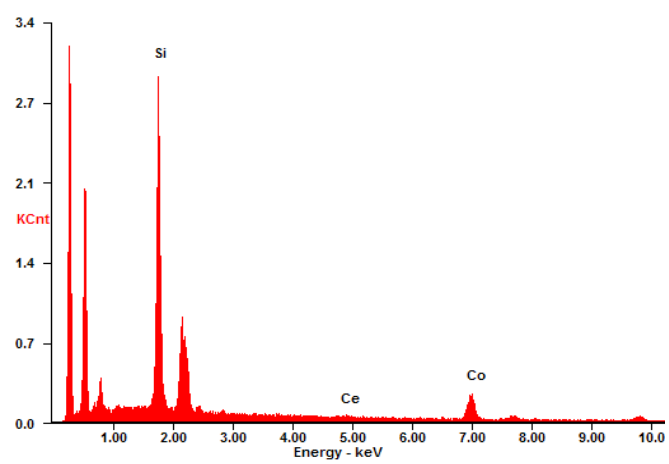
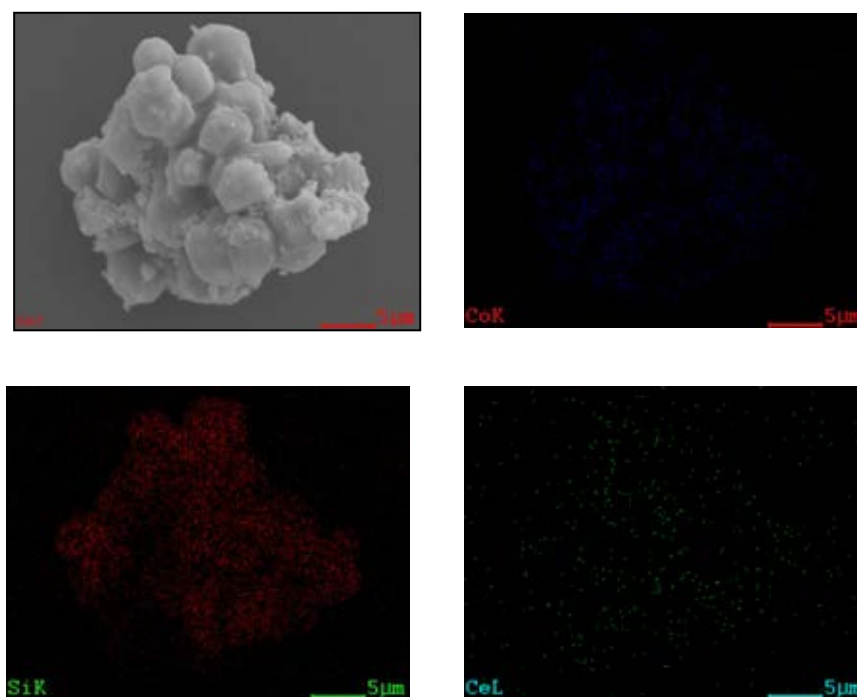
Element	Wt%	At%
SiK	62.56	81.24
CeL	12.30	03.20
CoK	25.14	15.56
Matrix	Correction	ZAF

Figure A.11 The SEM/EDX result of Co-Ce /SBA-15-V



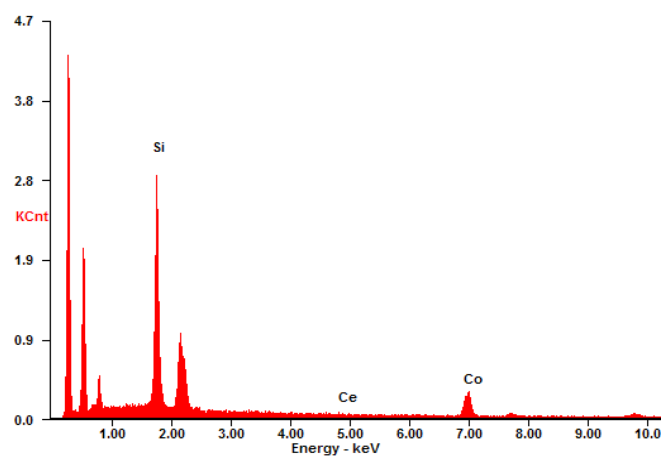
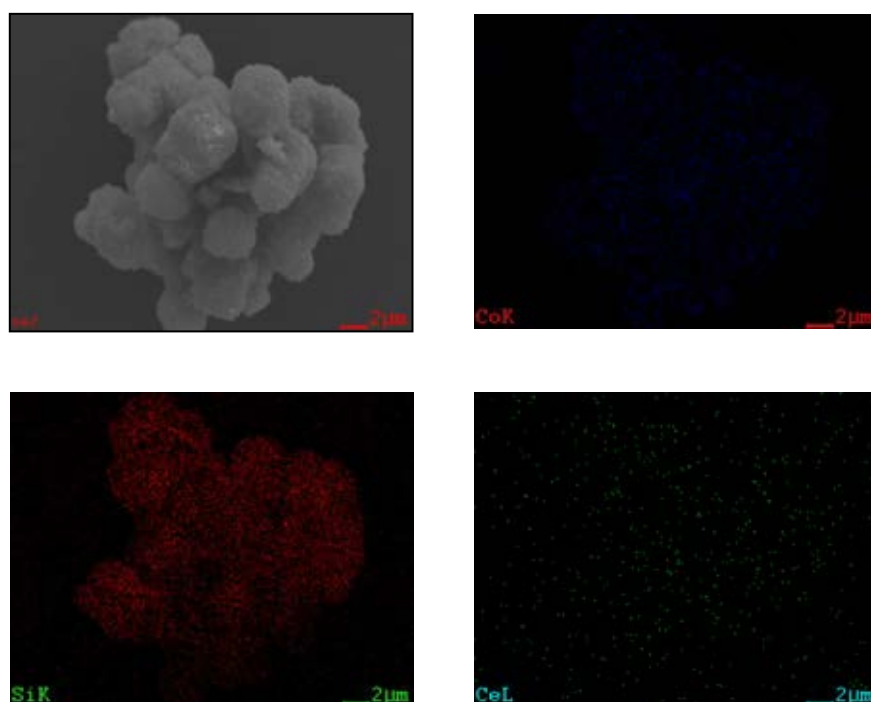
Element	Wt%	At%
SiK	45.25	67.19
CeL	14.49	04.31
CoK	40.27	28.50
Matrix	Correction	ZAF

Figure A.12 The SEM/EDX result of Co/Ce -SBA-15-V



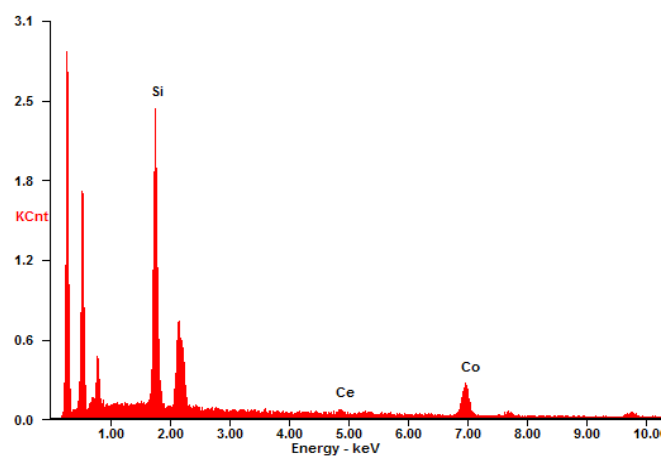
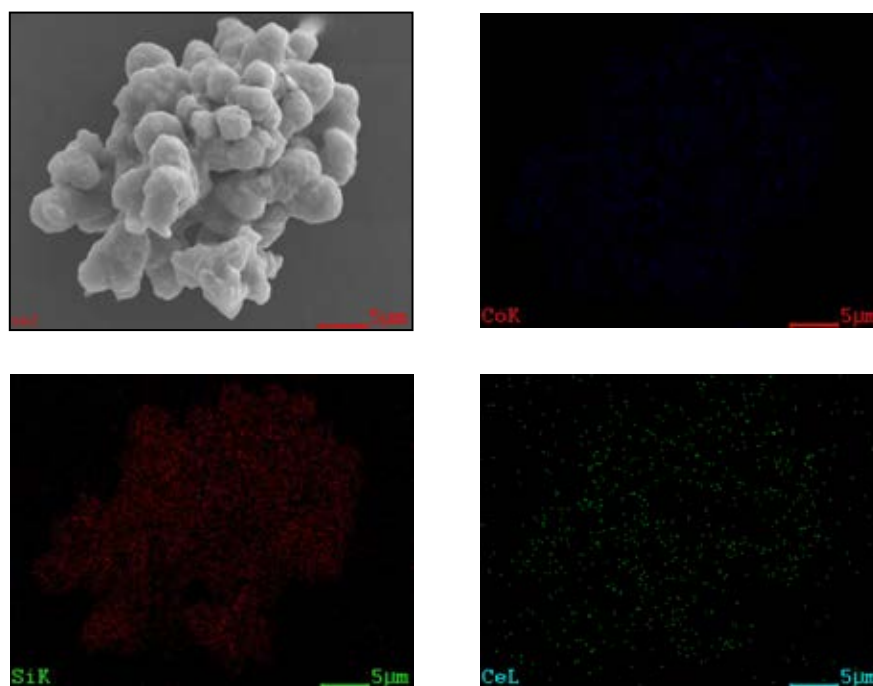
Element	Wt%	At%
SiK	47.46	68.50
CeL	11.66	03.37
CoK	40.88	28.12
Matrix	Correction	ZAF

Figure A.13 The SEM/EDX result of Co-Ce /SBA-16-N



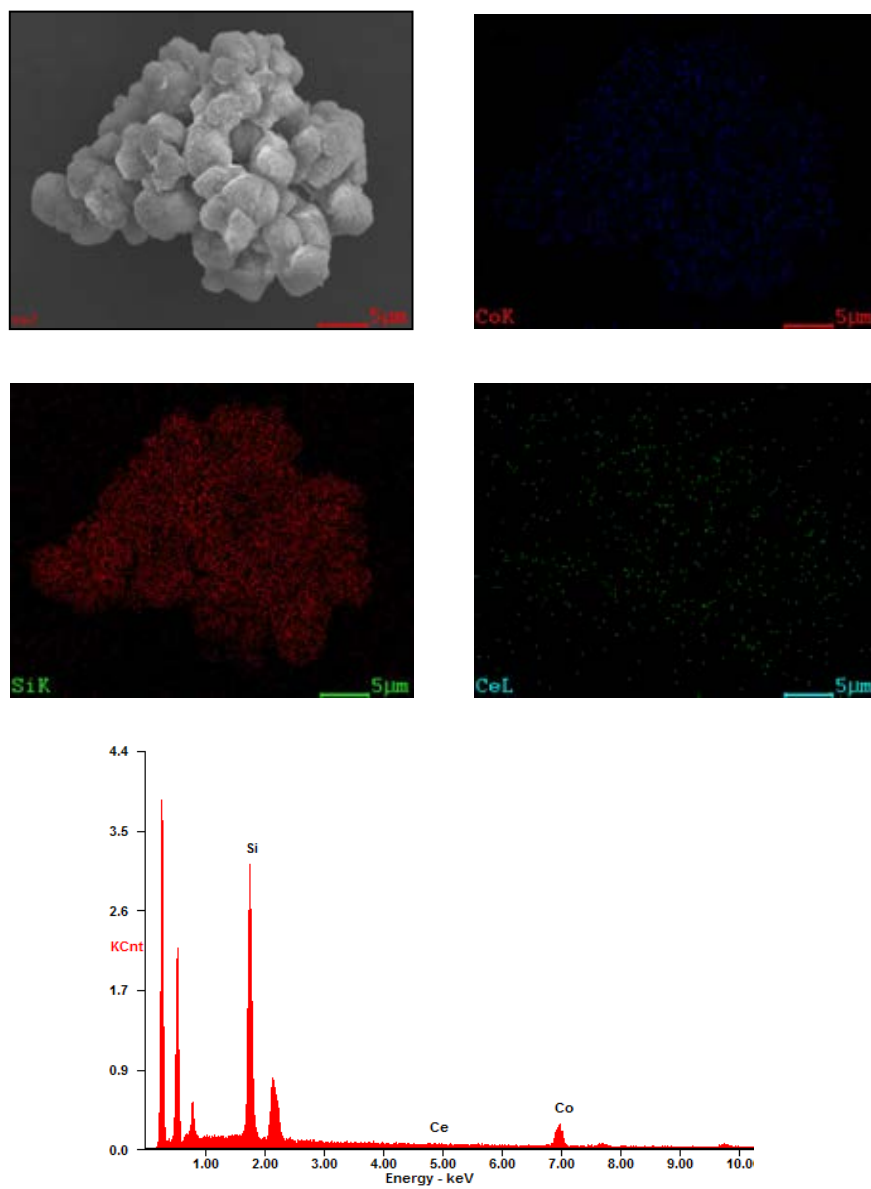
Element	Wt%	At%
SiK	47.81	67.47
CeL	06.59	01.86
CoK	45.60	30.66
Matrix	Correction	ZAF

Figure A.14 The SEM/EDX result of Co/Ce -SBA-16-N



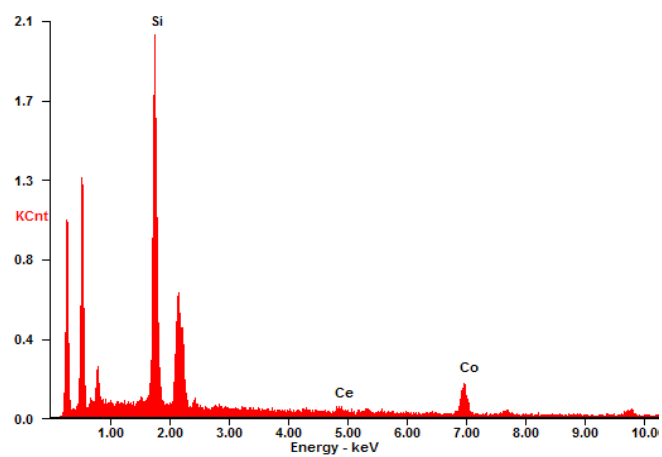
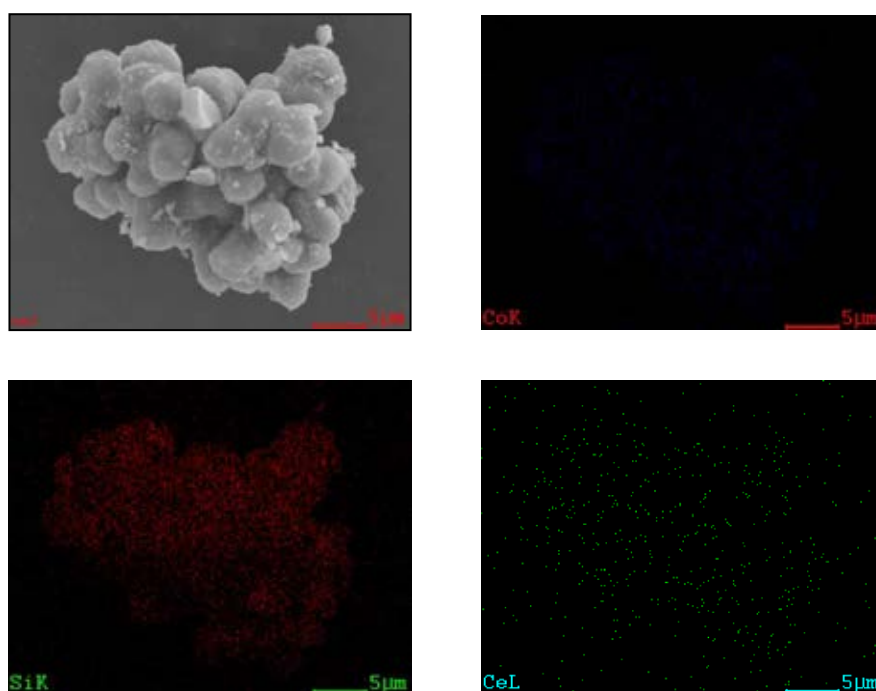
Element	Wt%	At%
<i>SiK</i>	43.93	65.46
<i>CeL</i>	12.82	03.83
<i>CoK</i>	43.25	30.72
<i>Matrix</i>	Correction	ZAF

Figure A.15 The SEM/EDX result of Co-Ce /SBA-16-U



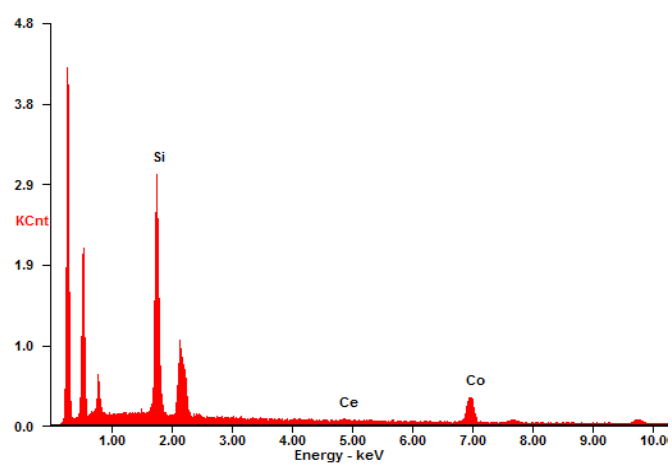
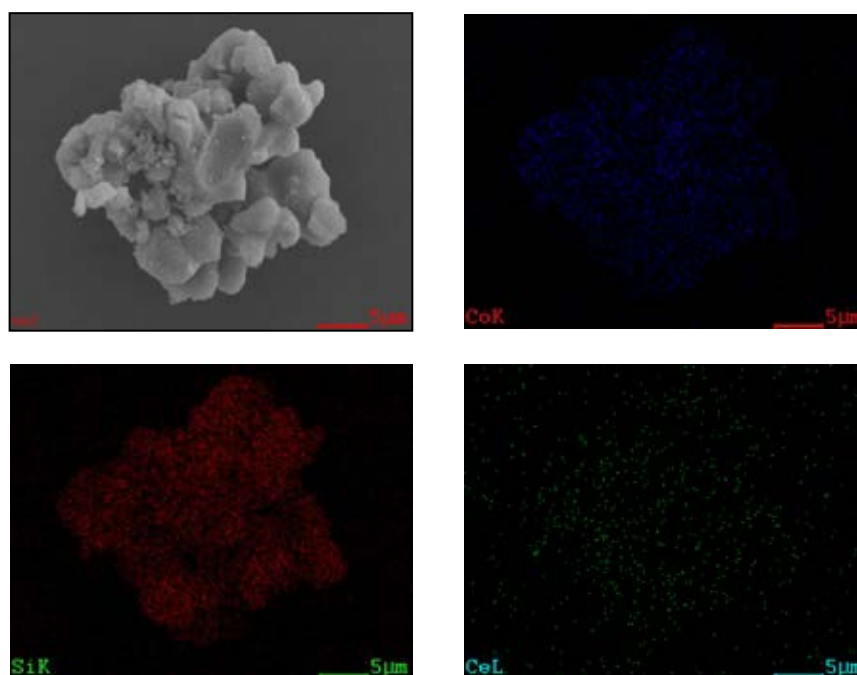
Element	Wt%	At%
SiK	50.47	69.95
CeL	06.96	01.93
CoK	42.57	28.12
Matrix	Correction	ZAF

Figure A.16 The SEM/EDX result of Co/Ce-SBA-16-U



Element	Wt%	At%
SiK	48.43	69.52
CeL	12.09	03.48
CoK	39.48	27.01
Matrix	Correction	ZAF

Figure A.17 The SEM/EDX result of Co-Ce /SBA-16-V



Element	Wt%	At%
<i>SiK</i>	47.23	67.90
<i>CeL</i>	10.22	02.95
<i>CoK</i>	42.55	29.15
<i>Matrix</i>	Correction	ZAF

Figure A.18 The SEM/EDX result of Co/Ce -SBA-16-V

APPENDIX C

GC CALIBRATION

This appendix describes the calibrations performed to reveal the results from the chromatograms. The calibrations were conducted from the two GC detectors. The first GC was used to quantify CO and CO₂ using the thermal conductivity detector. The second GC was used to quantify CH₄ and larger hydrocarbon using flame ionization detection. Four different compositions were examined in creating the curve standard. Figure A.19 and A.20 show the area under the peak of CO₂ and CH₄. Referring to area under the peak, the calibration curves for CO₂ and CH₄ can be calculated. Figure A.21 and A.22 show the calibration curves.

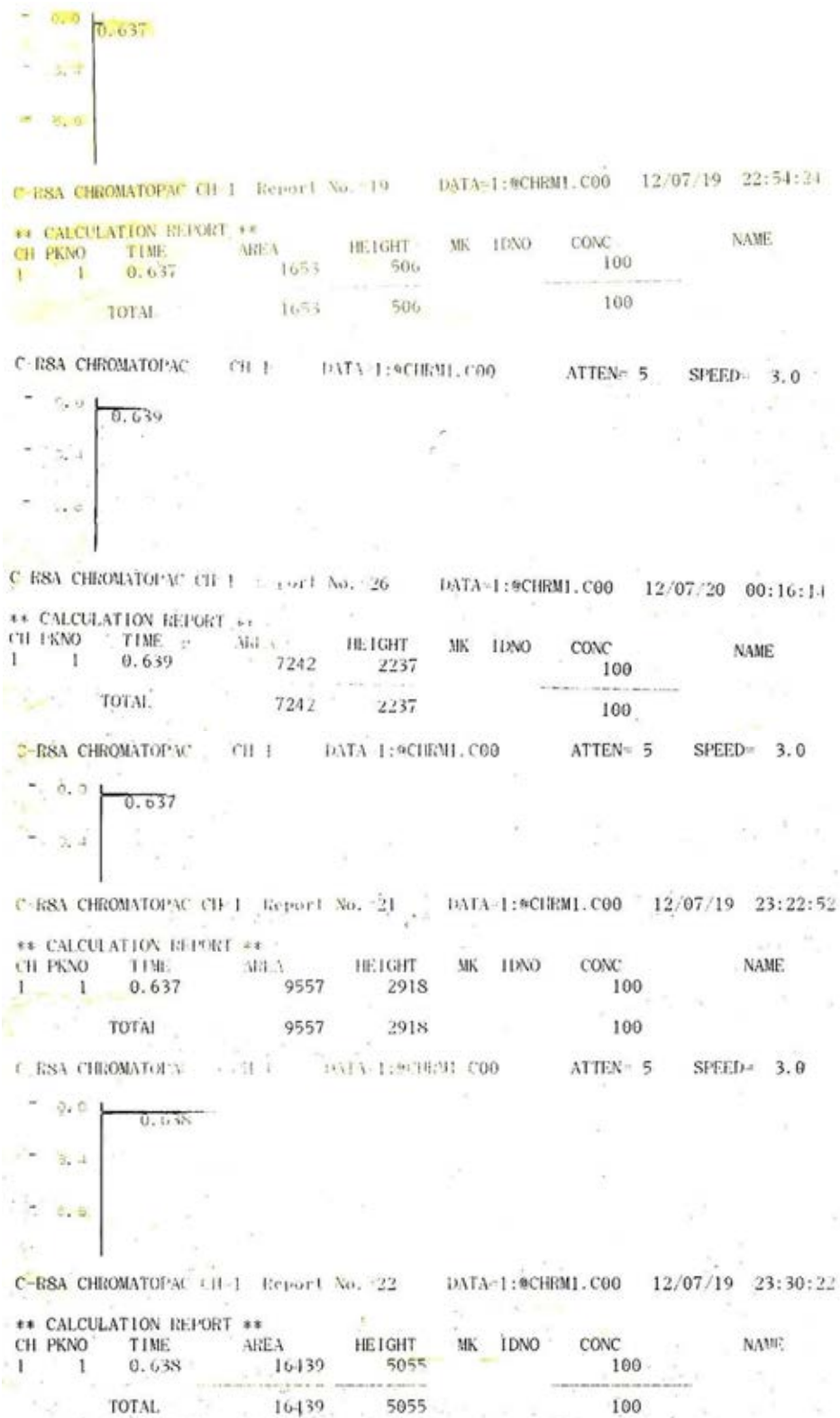


Figure A.19 The area under the peak of CO₂

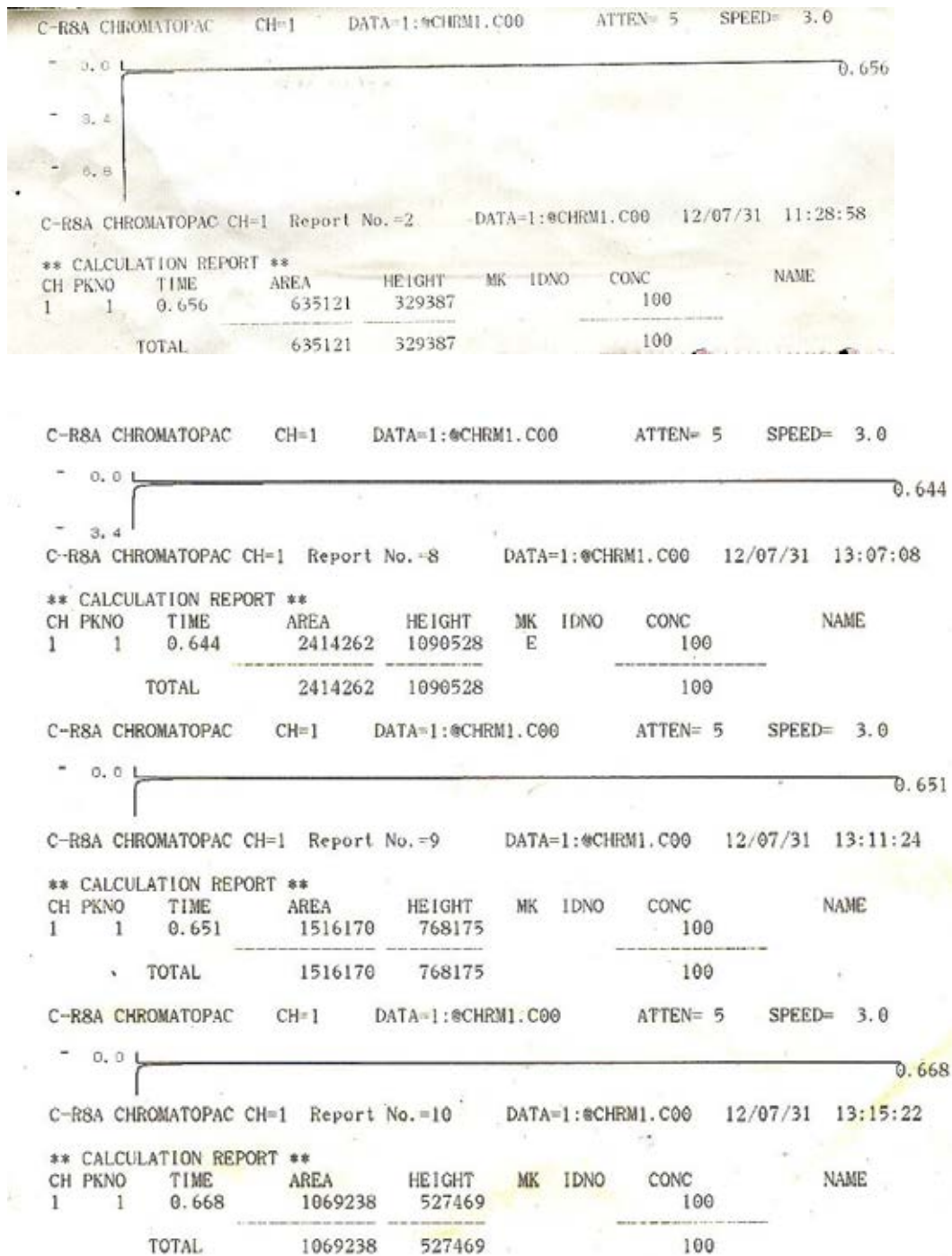


Figure A.20 The area under the peak of CH₄

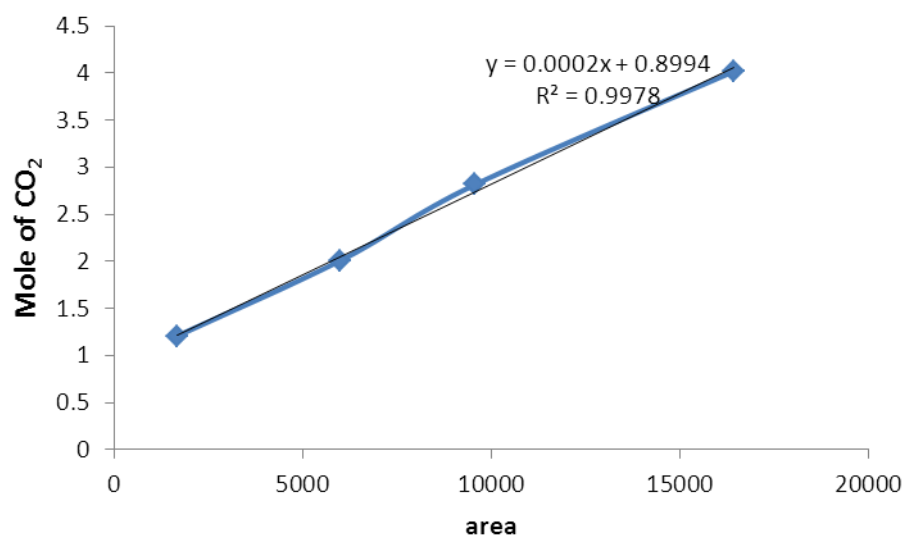


Figure A.21 The calibration curve for CO₂

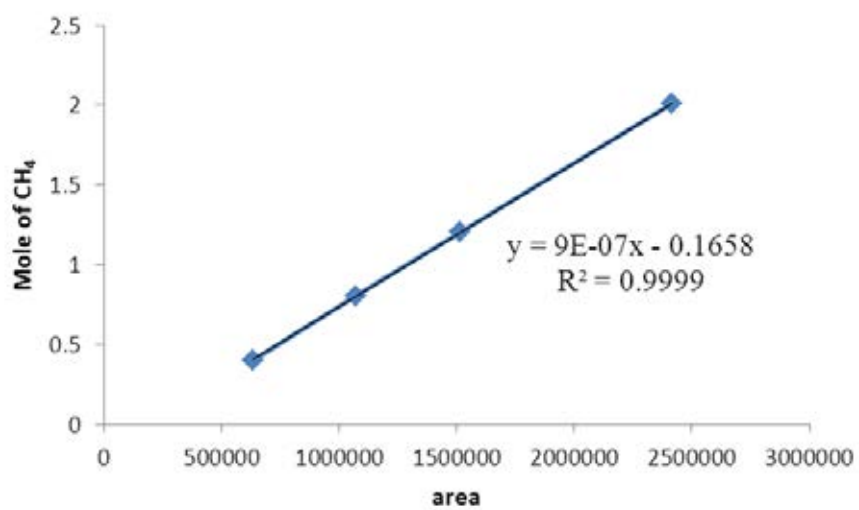
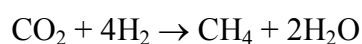


Figure A.22 The calibration curve for CH₄

APPENDIX D

CALCULATION OF CONVERSION AND REACTION RATE

Since all most 99% of product is methane, CO₂ conversion can be calculated conversion from CO₂ hydrogenation rate equation. One mole of CH₄ produced is equal to one mole of reacted CO₂. Calculation of conversion is displayed below.



$$\text{Conversion (\%)} = \frac{100 \times [\text{mole of CO}_2 \text{ in feed} - \text{mole of CH}_4 \text{ in product}]}{\text{mole of CO}_2 \text{ in feed}}$$

The rate of reaction can be determined based on conversion, which is shown below.

The weight of catalyst used	=	W	g
CO ₂ flow rate	=	2	cc/min
Reaction time	=	60	min
Weight of CH ₂	=	14	g
The volume of 1 mole gas at 1 atm	=	22400	cc

$$\text{Reaction rate} \left[\frac{\text{g CH}_2}{\text{g of catalyst}} \right] = \frac{\left[\frac{\% \text{conversion}}{100} \right] \times 60 \times 14 \times 2}{W \times 22400}$$

VITAE

Jittraporn Kruatim

Personal information

Date of birth: 24/02/1989

Place of birth: Bangkok/Thailand.

Email: kruatim.j@hotmail.com

Education

2010-2013 M. Eng., in Chemical Engineering Chulalongkorn University

- Thesis title : CO₂ hydrogenation over Co/SBA-15 and Co/SBA-16 promoted with ceria
- Received NRU scholarship (National Research University)

2006-2010 B.Sc., in Chemical Technology Chulalongkorn University

- Project title : Nano-fiber as heterogeneous catalyst

Conference

Characteristics of Co/SBA-15 and Co/SBA-16 catalysts prepared from different impregnation methods, The 2nd Nong Khai campus Conference 2012, Nong Khai/Thailand, 30-31 August 2012